Applied Catalysis B: Environmental 337 (2023) 122919

Contents lists available at ScienceDirect

Applied Catalysis B: Environmental

journal homepage: www.elsevier.com/locate/apcatb

Imprinting defective Fe-based metal-organic frameworks as an excellent platform for selective fenton/persulfate degradation of LEX: Removal performance and mechanism

Ying Zhao [b], Ruican Zhang [b], Jiamin Huang [b], Ying Zhang [b], Bo Han [c], Yupeng Ying [b], Min Chen [b], Shuyu Xie [a,b,*], Dongmei Chen [b,**]

[a] State Key Laboratory of Agricultural Microbiology Core Facility, China
[b] National Reference Laboratory of Veterinary Drug Residues (HZAU), Huazhong Agricultural University, Wuhan, Hubei 430070, China
[c] Faculty of materials science and chemistry, China university of geosciences, China

ARTICLE INFO

Keywords:
Imprinting defective MOF
Adsorption
Degradation
H_2O_2
Persulfate

ABSTRACT

Synergistic adsorption and advanced oxidation processes (AOPs) is being considered as an effective strategy to solve the poor catalytic performance and incomplete mineralization of pollutants currently faced by traditional AOPs and adsorption techniques. However, the poor adsorption-specificity/catalytic performance of catalyst needs to be improved. Herein, a daidzein imprinted defective Fe-MOF (Fe-MOF-DMIP) was successfully developed. Due to its enhanced hydrogen-bond/hydrophobic interaction and pore-filling effect, Fe-MOF-DMIP can selectively adsorb levofloxacin (Q_{max} was 315.31 mg g^{-1}). The acid-stability of Fe-MOF-DMIP in water was improved and pH can be expanded to 3–11. Attributed to the enhanced Fe cycle and mass transfer efficiency, Fe-MOF-DMIP could efficiently active H_2O_2/persulfate, resulting in the removal rate of levofloxacin reached 98.4%/82.4% (H_2O_2/persulfate). The synergistic mechanism of adsorption@degradation and degradation pathway were also expounded. This work provided a new strategy for developing multifunctional catalysts, and emphasized the importance of paying attention to the types of free radicals produced in AOPs.

1. Introduction

For a long time in the past, due to its excellent enrichment ability and economical use cost, adsorption technology has been widely used in water environment purification [1,2]. However, adsorption technologies are limited by their inability to fully mineralize emerging persistent pollutants such as pharmaceuticals and personal care products (PPCPs). In recent decades, because of their strong oxidizing capacity and high efficiency for degradation of PPCPs, advanced oxidation processes (AOPs) including Fenton oxidation and persulfate (PS) oxidation have been widely studied in the remove of PPCPs [3–5]. In general, the use of PS in AOP activated systems (including thermally activated systems [6–8], UV activated systems [9–11] and chemically activated systems [12,13]) showed great improvement in the reaction stoichiometric efficiency (RSE) compared to H_2O_2. The efficiency of catalyzing and utilizing reactive oxygen species (ROS, such as $SO_4^{\bullet-}$, •OH, $O^{2\bullet-}$ and $^1O^2$), generated instantaneously via activating H_2O_2/PS by catalysts, have been considered as two key factor affecting degradation performance of Fenton/PS oxidation. Due to the low toxicity and wide availability of iron, it was used as stand-alone material either in monometallic or multi-metallic systems to remove PPCPs through adsorption and sequestration into the nascent iron oxides species formed in situ in aqueous medium [14–18]. Later on, iron use has been improved by using it as semi-catalyst in AOPs [19–21]. However, the AOPs based on the iron-based catalyst still has some drawbacks, primarily including inefficient pollutant enriching ability, unsatisfactory oxidant utilization efficiency, leaching of metal ion and strict pH limitation (pH 3.0–5.0) (especially in Fenton oxidation), which may increase the cost of purification, and pose potential health risks to human and ecological environment [22–24].

Currently, synergistic adsorption and AOPs technologies have been developed to remove pollutants from water environment [25]. In this collaborative strategy, pollutants are firstly enriched on the surface of catalyst by adsorption, then the ROS generated on the surface of catalyst

* Corresponding author at: State Key Laboratory of Agricultural Microbiology Core Facility, China.
** Corresponding author.
E-mail addresses: snxsy1@126.com (S. Xie), chendongmei@mail.hzau.edu.cn (D. Chen).

https://doi.org/10.1016/j.apcatb.2023.122919
Received 21 January 2023; Received in revised form 22 May 2023; Accepted 24 May 2023
Available online 3 June 2023

directly acts on the enriched pollutants, which greatly improves the utilization efficiency of ROS, and solves the disadvantages of incomplete mineralization of pollutants by adsorption method. Obviously, catalyst in that strategy is required to have excellent adsorption capacity and catalytic capacity. Recently, due to their high specific surface area, especially its structure containing a large number of potential Fe active sites and well-dispersed pores in frameworks, Fe-MOF and their derivatives has shown potential application in the field of Fenton/PS oxidation [4]. Recent work showed PPCPs degradation in MIL88A/PS systems with high efficiency, however the physical properties of the probes in terms of adsorption affinity with the MOF played crucial role in the degradation process extent [12,13]. One of the significant reasons is that the microporous channels (< 2 nm) of Fe-MOF are not conductive to enriching small molecular PPCPs. In addition, the catalytic potential of Fe-MOF has not been fully released because a large number of metal active sites in the MOF framework are occupied by ligands, which seriously prevents Fe from catalyzing H_2O_2/PS to produce ROS. Due to the enhanced metal active sites, improved energy efficiency and low toxic metal dissolution, constructing mesoporous Fe-MOF catalysts with crystal defects is considered to be a more promising strategy [1,4,26,27]. Recently, introducing chemical regulators and high temperature activating are two common ways to construct defective Fe-MOF as catalysts [4,28]. However, defective Fe-MOF constructed by the above strategy still faces the disadvantage of insufficient selectivity for target pollutants and relatively narrow application range of pH. Because of the complex substrate of the water environment [29–32], ROS cannot achieve targeted degradation of target pollutants, if the adsorbent is non-selective. In addition, it is not unrealistic to adjusting the pH value of sewage environment to meet the degradation conditions. Therefore, it is an effective measure to improve the synergistic adsorption and oxidative degradation of water purification by putting forward a suitable construction strategy to prepare the defective Fe-MOF catalyst with high selective adsorption capacity, enhanced pH stability and high catalytic performance in water environment purification.

Molecularly imprinted polymers (MIPs), known as "artificial antibodies", are the most reported materials with specific ability to recognize target compounds, which could specifically generate molecular cavity with high binding affinity and prominent selectivity towards target molecules, and exhibit outstanding specificity for template molecules (usually target compounds) [33,34]. Although the low mass transfer efficiency and poor adsorption capacity severely hinder the further application of MIPs [35], but in our opinion, molecularly imprinted technology (MIT) could be introduced into the Fe-MOF synthesis system in the following ways to construct a defective imprinting Fe-MOF catalyst with excellent selectivity to target pollutants and enhanced catalytic performance: In the synthesis process, template is added to the synthesis system (containing reaction solution, metal ion and organic ligand) of Fe-MOFs to bind with metal ions and occupy some coordination sites of organic ligands. After proper elution of template, the metal active sites that bound to the template are exposed and formed defects. The Fe-MOF defect can serve as an enhanced stable active site for the catalysis of H_2O_2/PS. Therefore, defective imprinting Fe-MOF prepared based on MIT is expected to further release the high catalytic capacity of Fe-MOF to achieve specific targeted removal of pollutants in water environment. In addition, in order to avoid secondary pollution caused by template molecular leakage, it seems more reasonable to select environmentally friendly compounds with similar structure to target pollutants as virtual templates to prepare defective imprinting Fe-MOF.

In view of this, a virtual imprinting defective Fe-MOF (named as Fe-MOF-DMIP) with significantly enhanced pollutant target adsorption performance and efficient oxidant catalytic capacity were successfully synthesized by one-step solvothermal method. In this work, levofloxacin (LEX) was selected as a target pollutant owing to its potential harmfulness to human beings and aqueous environment. Correspondingly, after the database screening and comparison, daidzein (the structural analogue of LEX) was selected as the virtual template molecule. The objectives of this work include the following aspects: (I) studying the effect and mechanism of introducing daidzein into Fe-MOF-DMIP on selective adsorption of LEX; (II) exploring the role of daidzein in reducing Fe-MOF to form defective crystals; (III) studying the effect, degradation pathway and degradation mechanism of LEX removal by synergistic adsorption and degradation technology based on imprinting defective Fe-MOF-DMIP. In addition, although the efficiency of ROS production and utilization has proved to be important, when the concentration of ROS produced by same catalyst in different AOPs is similar and the types are different, whether the degradation performance of the same pollutant will be different, and what is the reason for this difference? This question doesn't seem to attract people's attention. Clearly, revealing this problem can provide valuable information for choosing the right AOP based on pollutant and catalysts. Therefore, in all the degradation tests of LEX mentioned above, we carried out synergistic adsorption and degradation technology based on both Fenton and PS oxidation, and tried to answer the above questions. To the best of our knowledge, this is the first report on the synergetic adsorption and degradation of organic pollutants by Fenton/PS oxidation that based on the imprinting defective Fe-MOF. It is reasonable to believe that our work will provides profound insight for constructing a multifunctional catalyst with both strong selective adsorption and catalytic performance, also provides a valuable reference for the correct selection of AOPs.

2. Experiments and methods

2.1. Reagents and chemicals

The reagents and chemicals used are listed in Supplementary Information (SI) (Text S1).

2.2. Methods

2.2.1. Preparation of Fe-MOF and Fe-MOF-DMIP

Fe-MOF and Fe-MOF-DMIP were prepared by one-step solvothermal method, as shown in Fig. S1. Firstly, Fe-MOF was prepared following the previously published work with some modification [36]. Briefly, 0.27 g (1.00 mmol) $FeCl_3{\cdot}6\ H_2O$ and 0.18 g (1.00 mmol) NH_2-BDC were dissolved in 40 mL DMF. The mixed solution was then transferred into a round-bottomed flask and heated up to 110 ℃ with gentle stirring for 24 h. After the reaction, the round-bottomed flask was cooled to room temperature, and the brown solid was rinsed with DMF and methanol to remove the unreacted precursor of material. Finally, the product (named as Fe-MOF) was obtained by rotary evaporation treatment under vacuum condition for 1 h.

The Fe-MOF-DMIP was prepared with the solvothermal method. After $FeCl_3{\cdot}6\ H_2O$ (1.00 mmol) and 0.50 mmol daidzein (DAN) was mixed in 40 mL DMF and vigorously stirred for 12 h, NH_2-BDC (1.00 mmol) was added into mixed solution. Then the mixed solution was heated up to 110 ℃ and reacted 24 h in a round-bottomed flask with gentle stirring. After cooling to the room temperature, brown solid was obtained by centrifugation and washed several times with DMF and methanol, respectively. Finally, the production was obtained by rotary evaporation treatment under vacuum condition for 1 h.

The amount of virtual template had a remarkable influence on the removal performance of MOF-DMIP [1]. Low dosage of template molecules could not make full use of the pore in Fe-MOF to form imprinted cavities, while too many template molecules could lead to the expansion and collapse of the Fe-MOF structure. Therefore, in order to study the effect of the amount of DAN added, different molar amounts (0.10, 0.25, 0.50, 0.75 and 1.00 mmol) of DAN were added to the synthetic system, and the resulting materials were labeled as Fe-MOF-DMIP-X (X = 0.10, 0.25, 0.50, 0.75 and 1.00), adsorption capacity, crystal structure and physicochemical properties were selected as optimization indexes.

2.2.2. Characterization

The structure and crystallinity of Fe-MOF/Fe-MOF-DMIP were characterized by X-ray diffraction (XRD, model D8 Advance). The morphology and mesostructured were performed by Field emission scanning electron microscope (FE-SEM) and transmission electron microscope (TEM). N_2 adsorption-desorption measurements were used to characteristic the specific surface area, pore volume and pore diameter of adsorbent. Fourier Transform infrared spectroscopy (FTIR) were used to investigate the chemical groups on the surface of adsorbent. In addition, X-ray photoelectron spectroscopy (XPS) was performed on the Fe-MOF-DMIP, to explore the formation mechanism and adsorption mechanism of Fe-MOF-DMIP and LEX in the aqueous solution.

2.2.3. Adsorption characteristics

Unless otherwise specified, the adsorption experiments were carried out in 250 mL transparent conical flask and placed in a thermostatic oscillator at 25 ℃ and with 180 rpm of oscillation rate. Each transparent conical flask contained 4 mg adsorbent, 150 mL of 10 mg/L LEX and solution without any adjustment.

For studying the LEX adsorption characteristics of Fe-MOF-DMIP, adsorption kinetics experiment, adsorption isotherm experiment, adsorption selectivity experiments and density functional theory (DFT) calculation were conducted. All the trial details of adsorption experiments can be found in the Text S1 of supplementary information (SI), and they were independently repeated at least three times, and error bars of the standard deviations and the average values are provided.

2.2.4. Catalytic degradation experiments

All the catalytic degradation experiments were conducted in 250 mL transparent conical flasks with 100 mL LEX solution (10 mg/L), 0.04 g L^{-1} of Fe-MOF/Fe-MOF-DMIP, and 0.5 mL 8 mM sodium persulfate (persulfate system) or 0.25 mL 30% H_2O_2 (Fenton system), under shaken at 25 ℃ and 180 rpm in dark.

In order to study the role of adsorption in degradation, the Fe-MOF-DMIP was added to LEX solution and oscillated for 1 h in the dark to achieve the adsorption equilibrium state. Then the oxidation reagent (H_2O_2/persulfate) was added to the suspension for catalytic degradation test, and 0.5 mL suspension was sampled into a 2 mL centrifugal tube containing 0.5 mL methanol (for quenching reaction) at 0, 15, 30, 60, 120 and 240 min, the samples were filtered with a 0.22 μm filter for detecting. A control group without the stage of adsorption was also conducted.

In the quenching experiments, tertiary butanol (TBA) was used as the quencher of •OH, ethyl alcohol (EA) was introduced to the solution as a scavenger of •OH and $SO_4^{\bullet-}$, isopropyl alcohol (IPA) was utilized to quench $SO_4^{\bullet-}$, Furfuryl alcohol (FFA) and benzoquinone (BQ) were often used to probe the formation of $^1O_2$ and $O_2^{\bullet-}$ [37,38].

2.2.5. pH stability, anti-interference capability, reusability and economic of Fe-MOF-DMIP

The effect of pH (3−10) in adsorption stage, co-existing ions (Cl^-, HCO_3^- and HPO_4^-) and humid acid (HA) in adsorption@AOPs were evaluated. Briefly, the coexisting inorganic anions solution (1–10 mM) and HA solution (0–30 mg/L) was added separately into the LEX solution (100 mL, 10 mgL^{-1}) in the Fenton/PS oxidation without pH adjustment.

The recycling testing both in adsorption alone and adsorption@AOPs were conducted, respectively. The Fe-MOF-DMIP after every cycle were separated through centrifugation, then added into the LEX solution with the same initial reaction conditions (H_2O_2/PS dosage, temperature and initial pH).

For the removal cost analysis of Fe-MOF-DMIP, we referenced previous study and made minor adjustments [9,39]. Briefly, we comprehensively considered the cost of raw materials (Fe^{3+}, NH_2-BDC and DAN et al.) required for the preparation of Fe-MOF-DMIP, the cost of raw materials (30% H_2O_2 or PS) required for adsorption@AOPs and the cost per use of Fe-MOF-DMIP after multiple cycles in 1000 L (1 m^3). Although our economic assessment is relatively crude, we believe that economic assessment can benefit the application of novel adsorbents/catalysts in environmental purification.

Detailed information on adsorption experiments, free radical species determination, HPLC analysis methods, electron paramagnetic resonance (EPR), mass spectrometry identification of degradation products and DFT calculations are provided in SI.

3. Results and discussion

3.1. Characteristic and comparing of Fe-MOF and Fe-MOF-DMIP

Various Fe-MOF-DMIP-X (X = 0.10, 0.25, 0.50, 0.75 and 1.00) materials were prepared by adding different dosage of DAN. According to the FE-SEM, TEM, XRD and TGA characteristics, as well as the evaluation of enrichment performance and N_2-adsorption-desorption analysis (Shown in Fig. (a)-(b) and SI (Text S2)), Fe-MOF-DMIP-0.5 was found to be in the best performance in the preliminary experiment. Therefore, the following characterization and comparative studies were conducted between Fe-MOF and Fe-MOF-MIP-0.5.

Firstly, the microstructure and morphology of Fe-MOF and Fe-MOF-DMIP were detected by FE-SEM and TEM, and the obtained images were shown in Figs. 1(c)-1(f). It can be seen that both Fe-MOF and Fe-MOF-DMIP showed regular octahedral structure, and there was no significant difference in particle size. However, comparing the surface smoothness of Fe-MOF and Fe-MOF-DMIP, Fe-MOF-DMIP showed significant roughness, while Fe-MOF was particularly smooth, indicating that the introduction of DAN did not lead to the apparent collapse of Fe-MOF-DMIP frame structure, while the coarser surface of Fe-MOF-DMIP indicated that there are defects on the crystal's surface. In addition, comparing the FTIR characterization results of Fe-MOF and Fe-MOF-DMIP (Fig. 1(g)), the stretching vibrations peaks of N-H and O-H in Fe-MOF-DMIP were shifted, which may be attributed to the introduction and complexation of phenolic hydroxyl groups in DAN. These results indicated that the introduction and appropriate elution of DAN could bring -OH to Fe-MOF-DMIP [40,41].

The lattice structures of Fe-MOF and Fe-MOF-DMIP were measured by XRD (Fig. 1(h)). It can be seen that the diffraction peaks of Fe-MOF-DMIP at 2θ were 9.17°, 10.13°, 16.56°, 18.20°, 20.36°, 24.57° and 28.85°, which was basically consistent with the diffraction peak of Fe-MOF at 2θ (9.17°, 10.13°, 12.93°, 16.56°, 18.20°, 24.57° and 29.09°). This was consistent with the diffraction peak reported in the previous research report [16,21], indicating that Fe-MOF was successfully synthesized, and the introduction of daidzein did not cause the collapsing of frame structural. However, the poor intensity of XRD diffraction peaks of Fe-MOF-DMIP indicated that there were defects in Fe-MOF-DMIP [4,42]. The decreased peak strength of Fe-MOF-DMIP was considered to be due to the introduction of DAN. Therefore, it can be furtherly concluded that the introduction of daidzein is conducive to the formation of defective Fe-MOF-DMIP.

Additionally, Thermogravimetric (TGA) analyses and X-ray photoelectron spectroscopy (XPS) characterization were also conducted to determine the type of formed defect of Fe-MOF-DMIP. As illustrated in Fig. 1(i), the weight loss between 30 and 100 °C was mainly due to the evaporation of water molecules. The second weight loss occurred in the range of 100 and 400 °C, mainly corresponding to the removal of anion ligands. While the third weight loss occurred in the range of 400 and 600 ℃, which may be attributed to the thermostable of organic ligands and daidzein. In the range of 400 and 600 °C, the mass decline rate of Fe-MOF-DMIP was lower than that of Fe-MOF with the calculated values of 21.27% and 23.52%, respectively, suggesting that there are missing ligands defects in Fe-MOF-DMIP. Furtherly, as shown in Fig. 1(j), full XPS spectra in the range of 0–1350 eV was given. The Fe/C ratio of Fe-MOF-DMIP was significantly lower than that of Fe-MOF, which was considered to be important evidence for determining the possible formation of

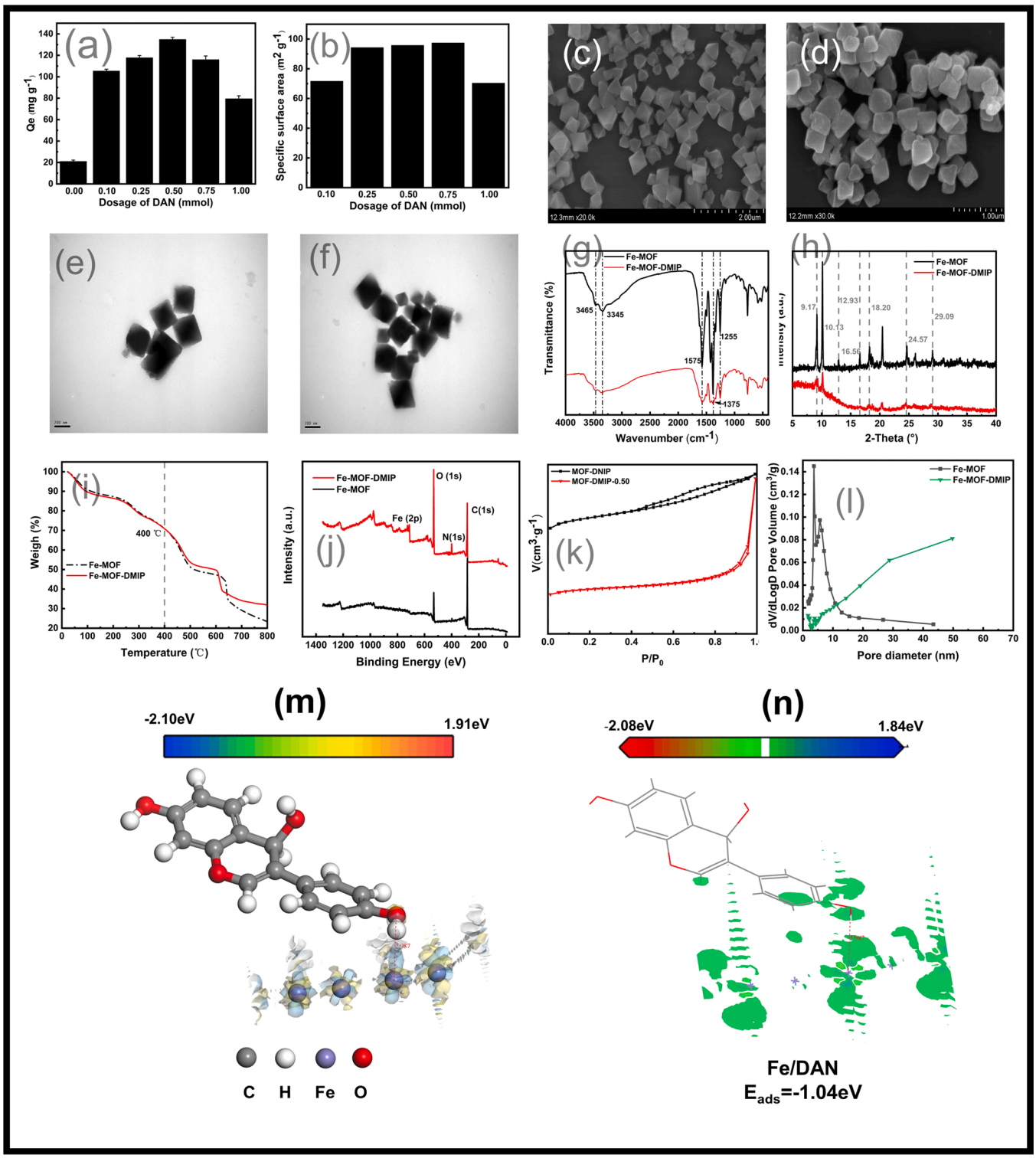

Fig. 1. The adsorption capacity with different dosage of template (a); The specific surface area with different dosage of template (b); SEM image of Fe-MOF (c) and Fe-MOF-DMIP (d); TEM image of Fe-MOF (e) and Fe-MOF-DMIP (f); FTIR spectrum of Fe-MOF and Fe-MOF-DMIP (g); XRD pattern of Fe-MOF and Fe-MOF-DMIP (h); N2 adsorption-desorption curve of Fe-MOF and Fe-MOF-DMIP (i); Pore distribution curve of Fe-MOF and Fe-MOF-DMIP (j); TGA curve of Fe-MOF and Fe-MOF-DMIP (k); XPS pattern of Fe-MOF and Fe-MOF-DMIP (l). Electron density difference model diagram of Fe/DAN(m); Binding energy of Fe/DAN(n).

missing ligands defects [4,43]. Therefore, according to the above results, it is reasonable to determine that the introduction and elution of daidzein can prepare defective Fe-MOF-DMIP of missing ligands.

Furtherly, the effect of introducing daidzein on the pore structure of Fe-MOF-DMIP was also analyzed by the result of N_2 adsorption/desorption measurement (Fig. 1(k)) and aperture distribution curve (Fig. 1(l)). The isotherm of Fe-MOF expectedly showed a mixture type I/II isotherm with a H1 hysteresis loop [44], indicating that the pore size distribution of the Fe-MOF was uniform. Moreover, it can be judged that the Fe-MOF-DMIP belongs to the IV type isotherm. A weak hysteresis loops was observed for Fe-MOF-DMIP, suggesting that the introducing of DAN changed the formation of mesoporous of Fe-MOF-DMIP [45].

Combined with the aperture distribution curve, the pore size of Fe-MOF was mainly concentrated around 3.66 nm, while the pore size of Fe-MOF-DMIP increased to 6.02 nm. Mesoporous pore is considered to be the ideal pore size for adsorption of antibiotic small molecules. Therefore, it is reasonable to judge that Fe-MOF-DMIP with mesoporous pores have good performance in the subsequent adsorption evaluation stage.

Furthermore, for clarifying the formation mechanism of Fe-MOF-DMIP, DFT calculation was used to construct adsorption model of Fe and chemical groups in DAN and calculate the charge differential density. As shown in Fig. 1(m), the calculated binding energy of Fe/DAN was negative (−1.04 eV), indicating that there was an interaction between DAN and Fe (III). Furtherly, the difference density of charge between DAN and Fe (III) was calculated. It can be seen from Fig. 1(n), among the 7-hydroxyphenyl, 4-hydroxyphenyl, carbonyl, and ether bonds of DAN, 4-phenol hydroxyl group showed significant electron cloud overlap with Fe (III), suggesting that daidzein was temporarily fixed in the Fe-MOF-DMIP channel by the coordination between 4-hydroxyl and Fe (III) coordination, and due to steric hindrance effect, the other groups that with lone pair electrons in DAN cannot coordinate with Fe (III). According to the above calculation results, we have reason to infer the formation process of Fe-MOFDMIP as follows: DAN was added into system and occupied some coordination site of Fe (III), which belongs to NH_2-BDC, through the coordination between 4-hydroxyl group and Fe (III). During the growth of Fe-MOF-DMIP crystals, due to the spatial structure of DAN, NH_2-BDC could only bind to the uncoordinated Fe (III) by bypassing DAN. Therefore, a spatial structure that was easier to accommodate DAN was formed in the pore of Fe-MOF-DMIP. Subsequently, after elution, the DAN was removed and the Fe (III) site chelated with 4-hydroxy was released and forming defects.

3.2. Adsorption characteristic of Fe-MOF-DMIP

3.2.1. LEX capture characteristics

Adsorption kinetics and adsorption isotherm were conducted to analyze the LEX capture characteristics of Fe-MOF-DMIP. For the adsorption kinetics study, it can be seen from Fig. 2(a), the adsorption rate of Fe-MOF-DMIP was fast in the first 20 min, reaching about 95% of the equilibrium adsorption amount. This is because a large number of adsorption sites in the initial stage of adsorption was vacant, which can efficiently identify and absorb LEX. Subsequently, the kinetic parameters and correlation coefficients (R^2) were given in Table S1. The R^2 of both pseudo-first-order model and the pseudo-second-order model were exceeding 0.9, indicating that the adsorption of LEX on Fe-MOF-DMIP is not a simple chemical adsorption or physical adsorption, but a combination of the two types of adsorption process [46]. In addition, according to the fitting results of intra-granular diffusion model (Fig. 2(b)), the adsorption process of LEX on Fe-MOF-DMIP included three phases, that determined by the intra-particle diffusion rate k (Table S1). Firstly, the focus point and the coordinate axis of the curve was not the origin, indicating that the intra-particle diffusion phase was not the only rate control step, surface adsorption also played an adsorption role [47,48]. The initial phase of the sharp rise within 15 min was due to the rapid migration of LEX molecules through solution diffusion to Fe-MOF-DMIP (known as external surface adsorption or transient adsorption). The subsequent step-up phase was attributed to the limited diffusivity within the particle. The final equilibrium stage was due to the relatively high sorbent saturation on the adsorbent surface and the extremely low concentration of LEX in the solution. Furthermore, the K_1 values were far higher than K_2 and K_3 values, indicating that the external film diffusion was a rate-controlled process.

Subsequently, adsorption isotherm (Fig. 2(c-f)) study was conducted and the isotherm parameters obtained from Langmuir and Freundlich models are presented in Table S2. The correlation coefficient of Langmuir and Freundlich models are both above 0.9, indicated that the

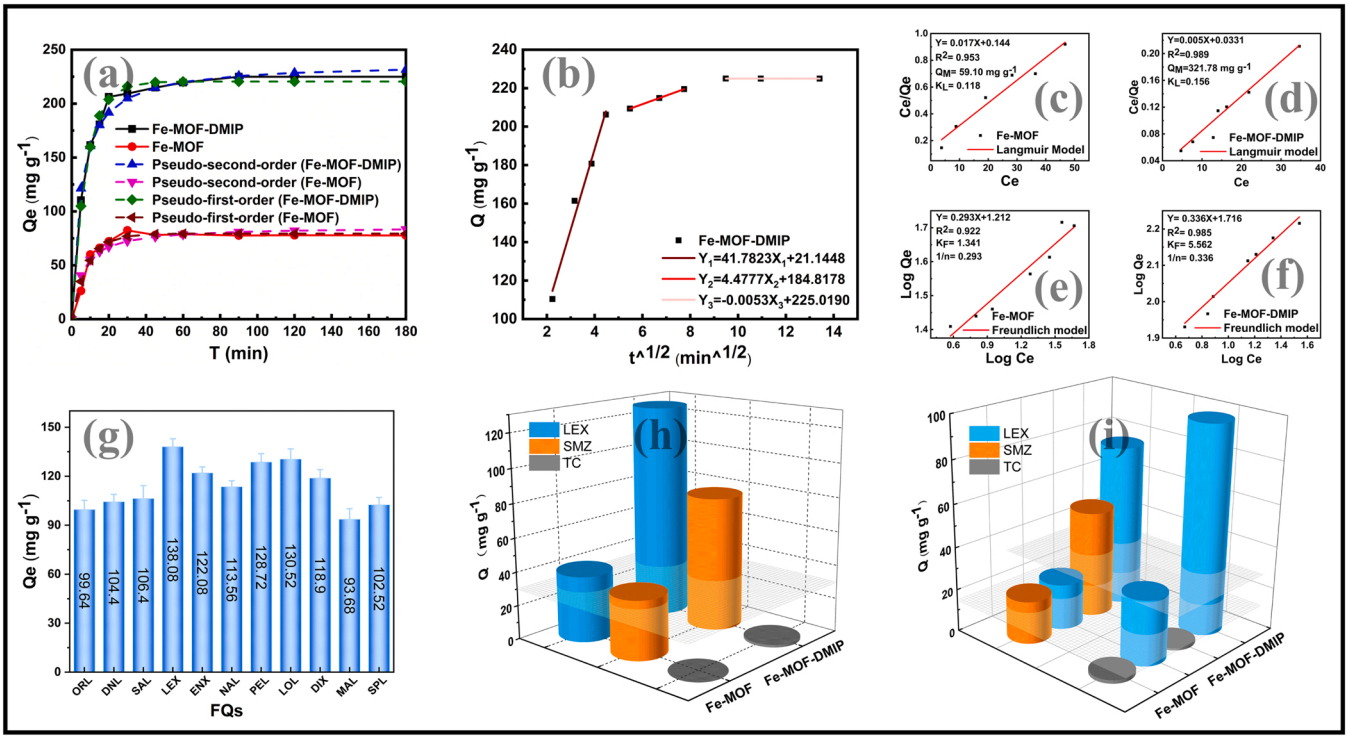

Fig. 2. The Pseudo-first-order and Pseudo-second-order model of Fe-MOF and Fe-MOF-DMIP (a); Intra-particle diffusion model of Fe-MOF-DMIP (b); Langmuir models and Freundlich models of Fe-MOF and Fe-MOF-DMIP (c-f); Adsorption capacity of Fe-MOF-DMIP for 11 FQs (g); Removal percentage of Fe-MOF-DMIP for 3 PFOAs (h); The result of unary selectivity test of Fe-MOF-DMIP (c); The result of binary selectivity test of Fe-MOF-DMIP (i).

adsorption of LEX is not monolayer chemical adsorption, but also multilayer physical and chemical adsorption [49]. In addition, the maximum adsorption capacity of 321.78 mg g^{-1} and minimum equilibrium adsorption time obtained by this work were higher than that of LEX adsorption studies previously reported (Table 1). These results suggest that the introduction of DAN leads to the multi-layered porous structure of Fe-MOF-DMIP, which can efficiently identify and capture LEX.

3.2.2. Adsorption selectivity

As beginning, single system adsorption test was conducted. That is, 11 fluoroquinolones (FQs) were configured in aqueous solution respectively. It can be found from Fig. 2(g) that the Fe-MOF-DMIP had great adsorption capacity on the 11 FQs studied (93.68–138.08 mg g^{-1}), among which LEX had the highest adsorption capacity on Fe-MOF-DMIP (138.08 mg g^{-1}) under experiment conditions. In addition, we studied the selective adsorption of LEX with competition compounds by Fe-MOF-DMIP in unitary system (TC, SMZ and Perfluoro-carboxylic acids (PFCAs)) and binary system (TC/LEX and SMZ/LEX). For the adsorption of three PFCAs (the mass spectrogram was given in Fig. S8), it can be seen from Fig. S9 that the adsorption capacity of three PFCAs onto both Fe-MOF-DMIP and Fe-MOF was very low, ranging from 0.004 to 0.121 mg g^{-1} and 0.006–0.019 mg g^{-1}, respectively. The results indicated that extended the pore size of Fe-MOF-DMIP by our strategy did not improve the adsorption capacity of PFCAs. For unitary selective adsorption test results (Fig. 2(h)), the adsorption capacity of LEX, SMZ and TC on Fe-MOF-DMIP were 126.89, 68.86 and 1.46 mg g^{-1}, respectively. And the adsorption capacity of LEX, SMA and TC on Fe-MOF were 28.82, 34.68 and 0.06 mg g^{-1}, respectively. The calculated imprinting factor (IF) of LEX, SMZ and TC were 4.40, 1.99, and 24.83, respectively. Moreover, the selectivity factor (β) of LEX/SMZ and LEX/TC were 2.21 and 0.18, respectively. According to the above results, it can be seen that Fe-MOF-DMIP had a better adsorption affinity on LEX than the other three competitive analogists. Moreover, due to the both low adsorption capacity of TC on Fe-MOF and Fe-MOF-DMIP, a slight change of the adsorption capacity of TC can lead to a significant change of the index of IF and β. Therefore, the introduction of daidzein was not considered to increase the adsorption affinity of Fe-MOF-DMIP to TC. In addition, as the spatial diameters of LEX and SMZ are all within the accommodating range of the Fe-MOF and Fe-MOF-DMIP, two adsorbents can accommodate a certain amount of LEX and AMX through pore filling effect (physical adsorption). However, the space structure of TC was too large to be accommodated by adsorbents.

Furthermore, the affinity of Fe-MOF-DMIP to LEX in the presence of competitors (SMZ or TC) was also studied by binary selectivity test. As illustrated in Fig. 2(i), the adsorption capacity (mg g^{-1}) of Fe-MOF-DMIP in LEX/SMZ and LEX/TC binary system was 96.45/46.15 and 98.09/1.00, respectively. The adsorption capacity (mg g^{-1}) of Fe-MOF in LEX/SMZ and LEX/TC binary system was 21.52/20.05 and 30.62/2.25, respectively. It can be seen that in the binary system, the adsorption capacity of Fe-MOF and Fe-MOF-DMIP for LEX and another analogue were both reduced, which could be attributed to the blockage of pore caused by the competitive of LEX and SMZ or TC. But obviously, the adsorption capacity of LEX on Fe-MOF was much less than that of Fe-MOF-DMIP. These results further proved that the introducing of DAN can significantly improve the adsorption selectivity of Fe-MOF-DMIP.

Table 1
Comparison of the adsorption performance of various adsorbents for OFX.

	Adsorption capacity (mg/g)	Equilibrium time (min.)	Ref.
Mesoporous carbon nanoparticles molecularly imprinted polymer	40.98	120	[50]
Rice husk ash	5.68–8.48	430	[51]
Mesoporous Al_2O_3, nonporous Al_2O_3, mesoporous SiO_2, nonporous SiO_2	0.8–1.5	30	[52]
Dissolved humic acid	0.09–1.02	-	[53]
Restricted access media-imprinted nanomaterials (RAM-MIPs)	80.64	15	[54]
Fe/Zn-H_3PO_4-sludge biochar	39.3	720	[55]
Fe-MOF-DMIP-0.5	321.78	20	This work

3.2.3. Adsorption mechanism of Fe-MOF-DMIP

In order to explore the mechanism of Fe-MOF-DMIP having excellent adsorption capacity and selectivity for LEX, the FTIR was used to analyze the changes of surface group of Fe-MOF-DMIP before and after adsorption, firstly. As shown in Fig. 3(a), the peak value at 628 cm^{-1} showed the stretching vibration of Fe-O before adsorption, and disappeared after adsorption [56]. In addition, a new band at 1930 cm^{-1} assigned to the C-N moiety was appeared (Xiang et al., 2020), suggesting that the N atom of LEX was involved in the adsorption. Perhaps due to the low materials content of F element in LEX, no C-F characteristic peak was observed near 1269 cm^{-1} [57]. After adsorption, we observed the deviation and weakened near 1500 cm^{-1} and 700 cm^{-1}, which could be attributed to COO^- stretching vibration formed by a characteristic peak of LEX-metal ion complex [57,58], which indicated that COO^- of LEX participated in the adsorption onto Fe-MOF-DMIP. Furthermore, there was a large absorption peak shifted at 3370 cm^{-1} after adsorption, which belongs to the stretching vibration peaks of -NH (NH_2-BDC) and -OH (NH_2-BDC and DAN) [1]. It is well known that -OH are the donors of hydrogen bond and -COO are the acceptors of hydrogen bond. Therefore, it was indicated that hydrogen bonding interaction was existed in the adsorption of LEX on Fe-MOF-DMIP. In addition, the hydroxyl shock peak of DAN near 3150 cm^{-1} was offset after adsorption [59], indicated that DAN provided binding sites for LEX adsorption by hydroxyl bond, furtherly.

To further verify the adsorption mechanism of LEX on Fe-MOF-DMIP, XPS was used to determine the elements of Fe-MOF-DMIP before and after adsorption. It can be seen from Fig. 3(b) and Fig. 3(c), the C (1 s) core level of C═O (288.71 eV) shifted to a lower binding energy (288.62 eV), and the binding energy for C-N of original Fe-MOF-DMIP was 290.70 eV, and the binding energy for C-N decreased (290.43 eV) after adsorption. In addition, the O (1 s) core level of Fe-O (530.65 eV) shifted to a lower binding energy (530.46 eV). The binding energy for Fe (2p-1/2) and Fe(2p-3/2) of original Fe-MOF-DMIP were 711.06 eV and 724.38 eV, respectively. After adsorption, the binding energy for Fe (2p-1/2) and Fe (2p-3/2) decreased to 710.86 eV and 724.02 eV, respectively, which might be attributed to the formation of coordinate bonds between LEX and Fe-MOF-DMIP, resulting in a decrease in charge density of Fe. This indicated that π-π conjugation and hydrogen bonding played an important role in the adsorption of LEX by Fe-MOF-DMIP. Moreover, the C (1 s) core level of C-O (286.28 eV) shifted to a lower binding energy (286.42 eV), and the O (1 s) core level of C-O (533.10 eV) shifted to a lower binding energy (533.42 eV), indicating that electrostatic attraction process existed in the adsorption of LEX by Fe-MOF-DMIP [57].

In addition, in order to reveal the influence of organic ligands (NH_2-BDC), metal ions (Fe) and template molecules (DAN) on LEX adsorption furtherly, the DFT was used to calculation the adsorption energies of NH_2-BDC/LEX, Fe/LEX and DAN/LEX (Table S3). According to the result, the adsorption energy of Fe/LEX was 1.24 eV, and the positive value indicated that the adsorption between Fe and LEX was not stable. However, the adsorption energy of NH_2-BDC/LEX was − 0.20 eV, indicating that NH_2-BDC played a dominant role in the adsorption of Fe-MOF for LEX. In addition, the adsorption energy of DAN for LEX was − 0.27 eV, indicating that the introduction of DAN in the preparation process of Fe-MOF-DMIP was conducive to the adsorption of LEX. In order to further clarify the role of each chemical group of each model, electron density difference calculation was carried out (Fig. 3(d) and

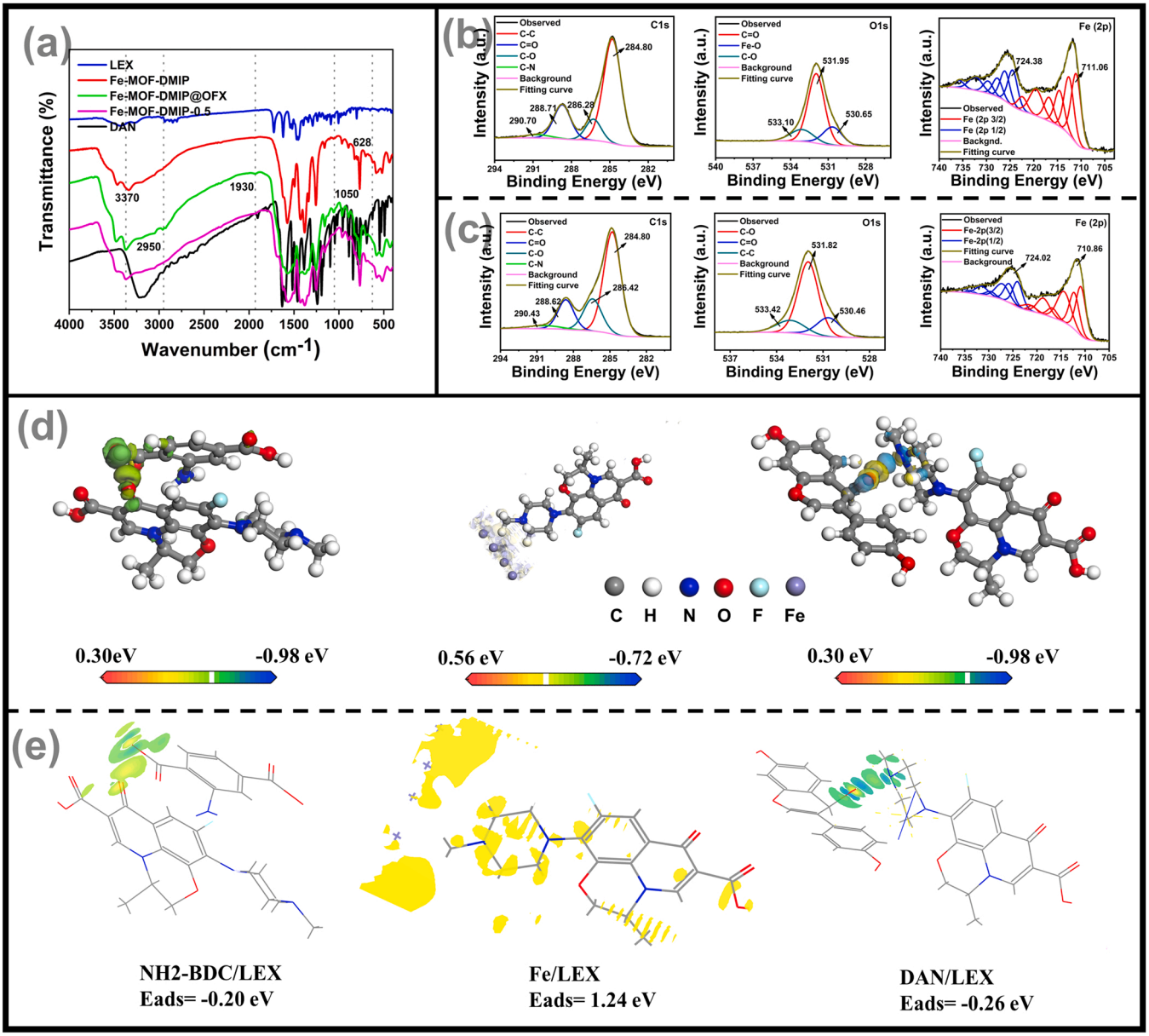

Fig. 3. FTIR spectra of Fe-MOF-DMIP before and after adsorption (a); XPS spectra of C (1 s), O (1 s) and Fe (2p) of Fe-MOF-DMIP before adsorption (b) and after adsorption (c); Electron density difference model diagram of NH_2-BDC/LEX, Fe/LEX and DAN/LEX (d); adsorption energy of NH_2-BDC/LEX, Fe/LEX and DAN/LEX (e).

Fig. 3(e)). The results showed that: (1) in the NH_2-BDC/LEX system, there was an obvious charge transfer between the 4-carbonyl group (LEX) and the carboxyl group (NH_2-BDC). (2) In the DAN/LEX system, there was an obvious charge transfer between N on piperazine ring (LEX) and 4-carbonyl (DAN).

In conclusion, NH_2-BDC and DAN played a dominant role in the adsorption of and LEX, which might be attributed to enhance π-π conjugation, hydrogen bond interaction and pore filling effect by the introduction of daidzein, resulting in higher adsorption selectivity and adsorption capacity of Fe-MOF-DMIP for LEX.

3.3. Catalytic study of Fe-MOF-DMIP

3.3.1. Advanced oxidation performance of Fe-MOF-DMIP

In this section, we compared the LEX removal performance of Fe-MOF and Fe-MOF-DMIP in the two most common AOPs (H_2O_2 and persulfate, equivalent to Fenton and PS). At the same time, the similarities and differences between Fe-MOF-DMIP/Fenton and Fe-MOF-DMIP/PS system were also compared to provide a reference for how to select appropriate AOPs according to different pollutants or catalyst.

Firstly, we carried out Fenton oxidation related experiments. As shown in Fig. 4(a), in the absence of Fe-MOF-DMIP, LEX removal efficiency by H_2O_2 reached the maximum at 120 min (22.3%). Due to the enhanced LEX enrichment capacity of Fe-MOF-DMIP, the removal efficiencies of Fe-MOF-DMIP reached 80.1% at 15 min, while that of Fe-MOF was 36%. In addition, the LEX.

removal rate of Fe-MOF-DMIP was 98.4% within 120 min, while the LEX removal rate of Fe-MOF was 53.0% within 120 min, indicating that the excellent adsorption performance and catalysis site of Fe-MOF-DMIP greatly improved the removal efficiency of LEX. This phenomenon was more obvious in the PS system. It can be seen from Fig. 4(b), LEX removal efficiency by persulfate along reached the maximum at 120 min (23.2%), while that of Fe-MOF/persulfate reached the maximum at

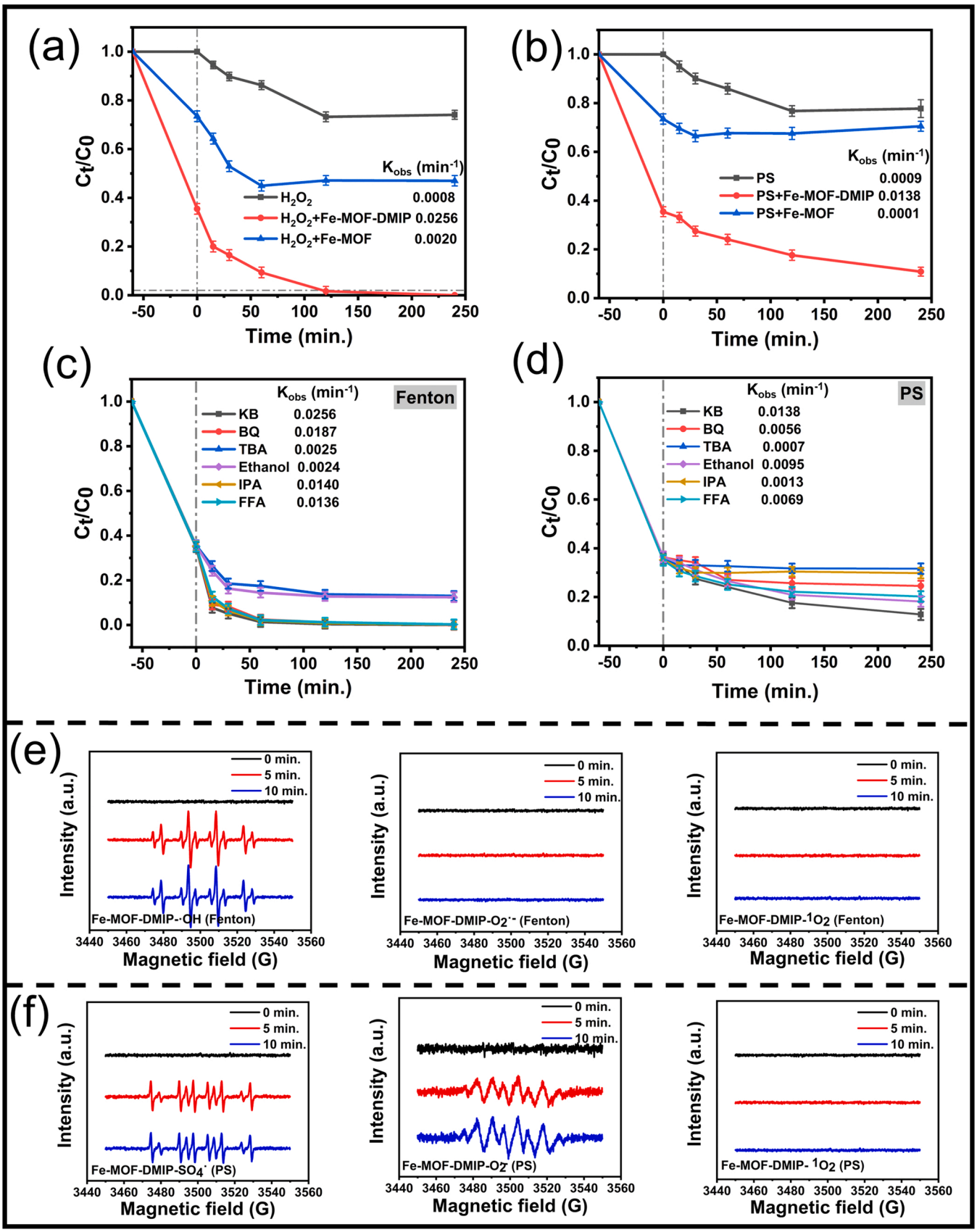

Fig. 4. LEX removal efficiency in Fe-MOF-DMIP/Fenton system (a); LEX removal efficiency in Fe-MOF-DMIP/persulfate system (b); removal of LEX with excessive scavengers in Fe-MOF-DMIP/Fenton system (c); removal of LEX with excessive scavengers in Fe-MOF-DMIP/persulfate system (d). EPR spectra in e-MOF-DMIP/Fenton system (e) and Fe-MOF-DMIP/persulfate system (f).

30 min (33.5%). The LEX removal rate of Fe-MOF-DMIP/persulfate reached 72.5% at 30 min, and reached 90.1% at 240 min. In addition, the parameter K_{obs} (Eq. S10) for LEX removal in H_2O_2, Fe-MOF/H_2O_2, Fe-MOF-DMIP/H_2O_2, PS, Fe-MOF/PS and Fe-MOF-DMIP/PS were calculated as 0.0008, 0.002, 0.0256, 0.0009, 0.001 and 0.0138 (min^{-1}), respectively. The above results indicated that the adsorption and AOPs of LEX based on Fe-MOF-DMIP are not additive, but synergistic.

In order to evaluate the catalytic activity of Fe-MOF-DMIP for H_2O_2/PS, RSE at 4 h degradation was calculated and compared with the reported study on the degradation of LEX by activation of PS. As shown in Table 2, the RSE of various catalysts (such as carbon-based materials, metal oxides and polymetallic composites et al.) that have been reported for LEX oxidative degradation ranged from 0.93% to 13.8%, much lower than the 63.9% of Fe-MOF-DMIP. This is mainly attributed to the high adsorption performance and catalytic efficiency of Fe-MOF-DMIP, indicated the catalyst prepared by MIT@MOF strategy has a broad application prospect in environmental purification.

3.3.2. Degradation mechanism

Firstly, the related ROS in the degradation process of LEX in Fe-MOF-DMIP/Fenton and Fe-MOF-DMIP/PS systems were explored, and the K_{obs} was calculated in the presence of FFA, BQ, TBA, EA and IPA, respectively (Table S4). As shown in Figs. 4(c)-4(d), in the presence of FFA (50 mM, $K^{1}_{O2)} = 1.2 \times 10^8\ M^{-1}{\cdot}S^{-1}$) [70], and BQ (50 mM, $K^{\bullet}_{O2-} = 9.0 \times 10^8\ M^{-1}{\cdot}S^{-1}$) [61], there was no significantly inhibitory effect on the degradation of LEX (with removal rates of 98.85% and 98.05% within 120 min, respectively), indicating $^1O_2$ and $O_2^{\bullet-}$ were not major ROSs in LEX degradation in Fe-MOF-DMIP/Fenton system. However, the elevated LEX degradation by Fe-MOF-DMIP was strikingly inhibited by adding TBA ($K_{(\bullet OH)} = 3.8–7.6 \times 10^8\ M^{-1}{\cdot}S^{-1}$, $K^{\bullet}_{SO4} = 4–9.1 \times 10^5\ M^{-1}{\cdot}S^{-1}$) [71] and EA ($K_{(\bullet OH)} = 1.9 \times 10^9\ M^{-1}{\cdot}S^{-1}$, $K^{\bullet}_{SO4} = 5 \times 10^7\ M^{-1}{\cdot}S^{-1}$), but insignificantly inhibited by IPA ($K^{\bullet}_{SO4} = 8 \times 10^7\ M^{-1}{\cdot}S^{-1}$) [72], suggesting that •OH was major ROS in Fenton oxidation (with removal rates of 86.30%, 87.25% and 99.2% within 120 min, respectively). In the Fe-MOF-DMIP/PS systems, the type of produced ROS was significantly different. The degradation of LEX was significantly inhibited when adding TBA, EA and IPA to the Fe-MOF-DMIP/PS system, respectively, indicating that •OH and $SO_4^{\bullet-}$ played a dominant role. In addition, the presence of BQ and FFA inhibited the degradation of LEX to some extent, suggesting $^1O_2$ and $O_2^{\bullet-}$ were involved in the degradation of LEX (with removal rates of 74.32% and 77.80% within 120 min, respectively). Subsequently, in-situ EPR was used to further identify and quantification related ROS, DMPO was used to capture the signals of •OH and $SO_4^{\bullet-}$, and TEMP was applied to trap the signals of $^1O_2$. It can be seen from Fig. 4(e), only •OH characteristic peaks (four-lines, 1:2:2:1) were indeed detected in Fe-MOF-DMIP/Fenton system. Meanwhile, the different intensity of •OH, $SO_4^{\bullet-}$ (six-lines, 1:1:1:1:1:1) and $O_2^{\bullet-}$ (seven-lines, 1:2:1:2:1:2:1) were detected in Fe-MOF-DMIP/PS (Fig. 4f). The spin concentration per unit volume (Fig. S10) of •OH detected in Fe-MOF-DMIP/Fenton system is 1.653 e^{12}, while •OH/$SO_4^{\bullet-}$ and $O_2^{\bullet-}$ detected in Fe-MOF-DMIP/PS system were 1.192 e^{12} and 3.633 e^{12}, respectively. It is known that $SO_4^{\bullet-}$ (2.5–3.1 V) has a higher redox potential than other free radicals (•OH is 1.8–2.7 V, $O_2^{\bullet-}$ is −0.56 V), and due to the higher electron affinity and lower O-O bond dissociation energy of $SO_4^{\bullet-}$, PS oxidation have been considered has higher activation efficiency than Fenton[73]. Furthermore, previous studies also suggested that catalysts containing higher mesoporous structures can shorten the migration distance of free radicals from active sites to the target pollutant and improve the mass transfer efficiency [5,41]. However, in this work, Fe-MOF-DMIP/Fenton system had a better removal effect of LEX than that of Fe-MOF-DMIP/PS system at similar free radical content, indicating there are other reasons for the different catalytic properties of Fe-MOF-DMIP in different systems.

According to the report of Kateřina et al., flavonoids and flavonoid compounds (such as daidzein) could promote the reduction of Fe (III) to Fe (II) by enhancing the production of •OH [74]. Therefore, one reason why the catalytic effect of Fe-MOF-DMIP was significantly improved in both Fenton and PS systems could be attributed to the fact that the introduction of DAN significantly improved the cycling efficiency of Fe (III)/Fe (II) and the generation rate of •OH. In addition, as shown in Eq. (1)(2)(3)(4)(5)(6)(7), self-coupling and cross-coupling reactions can occur between free radicals[75,76]. In Fe-MOF-DMIP/Fenton system, •OH can self-couple to produce H_2O_2 ($K_1 = 5.5 \times 10^{10}\ M^{-1}\ s^{-1}$), cross-couple with H_2O_2 to produce $O_2^{\bullet-}$ ($K_2 = 2.7 \times 10^7\ M^{-1}\ s^{-1}$), and cross-couple with $O_2^{\bullet-}$ to produce OH^- and $^1O_2$ ($K_3 = 8 \times 10^9\ M^{-1}\ s^{-1}$). This indicated that trace concentration $O_2^{\bullet-}$ was involved in the degradation of LEX, although $O_2^{\bullet-}$ was not detected by EPR (low-rate constant of K_2 limited the production of $O_2^{\bullet-}$). The coupling reactions in Fe-MOF-DMIP/PS systems were relatively complex. Firstly, the produced •OH can coupling reactions as Eq. (1)(2)(3). And, $SO_4^{\bullet-}$ can self-couple to produce $S_2O_8^{2-}$ ($K_4 = 7.6 \times 10^8\ M^{-1}\ s^{-1}$), cross-couple with $S_2O_8^{2-}$, H_2O_2 and •OH to produce $S_2O_8^{\cdot-}$, $HSO_4^{\cdot}$ and $HS_2O_5^{\cdot}$, respectively ($K_5 = 6.6 \times 10^5\ M^{-1}\ s^{-1}$, $K_6 = 1.2 \times 10^7\ M^{-1}\ s^{-1}$ and $K_7 = 1.0 \times 10^9\ M^{-1}\ s^{-1}$). In addition, the half-life of ROSs (•OH, $O_2^{\bullet-}$, $^1O_2$ and $SO_4^{\bullet-}$ were 10^{-9} s, >1 s, $2\sim4 \times 10^{-6}$ s and $3\sim4 \times 10^{-5}$ s, respectively [76-79]) is another parameter that should be taken into account. In both self-coupled and cross-coupled reactions, longer half-lives may result in more ROSs being consumed instead of being used to oxidize contaminants. Mutual scavenging of reactive oxygen species was more frequent in the PS system, various free radicals produced in Fe-MOF-DMIP/PS system showed antagonistic action in LEX degradation, but not synergistic action. This is consistent with the calculated K_{obs}, that is, under the condition of the same Fe-MOF-DMIP dosage and similar LEX removal rate, K_{obs} in Fenton (0.256 min^{-1}) was nearly twice that in the PS system (0.138 min^{-1}).

$$OH + \cdot OH \rightarrow H_2O_2 \quad (1)$$

$$\cdot OH + H_2O_2 \rightarrow O_2^{\cdot-} + H \quad (2)$$

$$\cdot OH + O_2^{\cdot-} \rightarrow {}^1O_2 + OH^- \quad (3)$$

$$SO_4^{\cdot-} + SO_4^{\cdot-} \rightarrow S_2O_8^{2-} \quad (4)$$

$$SO_4^{\cdot-} + S_2O_8^{2-} \rightarrow S_2O_8^{\cdot-} + SO_4^{2-} \quad (5)$$

$$SO_4^{\cdot-} + H_2O_2 \rightarrow HSO_4^{\cdot} + HO_2 \quad (6)$$

$$SO_4^{\cdot-} + \cdot OH \rightarrow HS_2O_5^{\cdot} \quad (7)$$

Furtherly, combined with the above speculation and the report of defective iron-based catalyst applied in AOPs, the main catalytic

Table 2
Comparison of RSE of Fe-MOF-DMIP with reported catalysts in LEX degradation.

Catalyst	Dosage of catalyst (mg)	Working pH	AOPs	RSE (%)	reference
NBH+Fe(III)	10 + 2 μmol	4.5	PMS	13.8	[60]
B/N-C@Fe	20	-	PMS	0.93	[61]
Fe_3O_4–CaO_2/NF	20	5.6	E-PMS	1.1	[62]
Ag/AgCl@ZIF-8/g-C_3N_4	50	6.5	VP-PMS	1.38	[63]
Co-Fe PBAs@rGO	5	5.5	PMS	13.18	[64]
Mo/Co HHBONs	5	7	PMS	2.77	[65]
PZBC800	10	6.55	PMS	4.43	[38]
ZIF-67/VTM	20	6.4	PMS	11.33	[66]
nZVI/CF-T-s	20	7.0	PMS	5.53	[67]
$CoFe_2O_4$/NF	-	7.0	E-PMS	1.10	[68]
NCS/NF	-	7.0	PMS	5.5	[69]
Imprinting defective Fe-MOF	4	7.0	PS	63.9	This work

(Note: E-PMS=electro PMS, VP-PMS=visible-light photocatalytic)

degradation process of LEX by Fe-MOF-DMIP in Fenton and PS system was described as follows (Eq.(8)(9)(10)(11)(12)(13)(14)), and the main LEX degradation mechanism in the Fe-MOF-DMIP/Fenton and Fe-MOF-DMIP/PS system were present in Fig. 5: firstly, in the system of Fe-MOF-DMIP/Fenton, Fe (III), functioned as an electron receptor, promoted the cleavage of H_2O_2 to generate Fe (II), and then Fe (II) reacted with H_2O_2 to generate •OH. Due to daidzein's reduction capacity, it promoted the conversion of Fe (III) to Fe (II) resulting in an increase of •OH on Fe-MOF-DMIP surface, and further shortening the migration of •OH to LEX and improving the utilization efficiency of •OH. While, in the system of Fe-MOF-DMIP/PS, the generate of ROS was relatively complicated. Fe (III) was reduced by HSO_5^- to form Fe (II), then $SO_4^{\bullet-}$ was generated via the reaction of Fe (II) with HSO_5^-, and $SO_4^{\bullet-}$ reacting with H_2O or OH^- generated •OH.

$$Fe\quad(III)+H_2O_2\rightarrow Fe\quad(II)+HO_2\cdot+H^+ \tag{8}$$

$$Fe\quad(II)+H_2O_2\rightarrow Fe\quad(III)+\cdot OH+OH^- \tag{9}$$

$$Fe\quad(III)@Daidzein\quad+H_2O_2\rightarrow Fe\quad(II)+HO_2\cdot+H^+ \tag{10}$$

$$Fe\quad(III)+HSO_5^-\rightarrow Fe\quad(II)+SO_5^{\bullet-}+H^+ \tag{11}$$

$$Fe\quad(II)+HSO_5^-\rightarrow Fe\quad(III)+SO_4^{\bullet-}+OH^- \tag{12}$$

$$SO_4^{\bullet-}+H_2O\rightarrow SO_4^{2-}+\cdot OH+H^+ \tag{13}$$

$$SO_4^{\bullet-}+OH^-\rightarrow SO_4^{2-}+\cdot OH \tag{14}$$

3.3.3. Degradation pathway

IT-TOF analysis was conducted to identify intermediates in LEX degradation formed by Fe-MOF-DMIP/Fenton and Fe-MOF-DMIP/persulfate. From the data (Fig. S11) and the Fukui index of the ROS attacking for LEX reported by Li et al. [80], there were three degradation pathways proposed in Fe-MOF-DMIP/Fenton system (Fig. 6a). In pathway I, the fluorine group was substituted with a hydroxyl group to form LEX-1. Subsequently, the quinolone ring was easily disrupted by ROS to produce compounds LEX-1.1 and LEX-1.2, while LEX-1.3 and LEX-1.4 were produced via demethylation of the amine side chain and dihydroxylation of the quinolone ring, respectively. In addition, the quinolone ring was further disrupted to form LEX-1.5 and LEX-1.6.

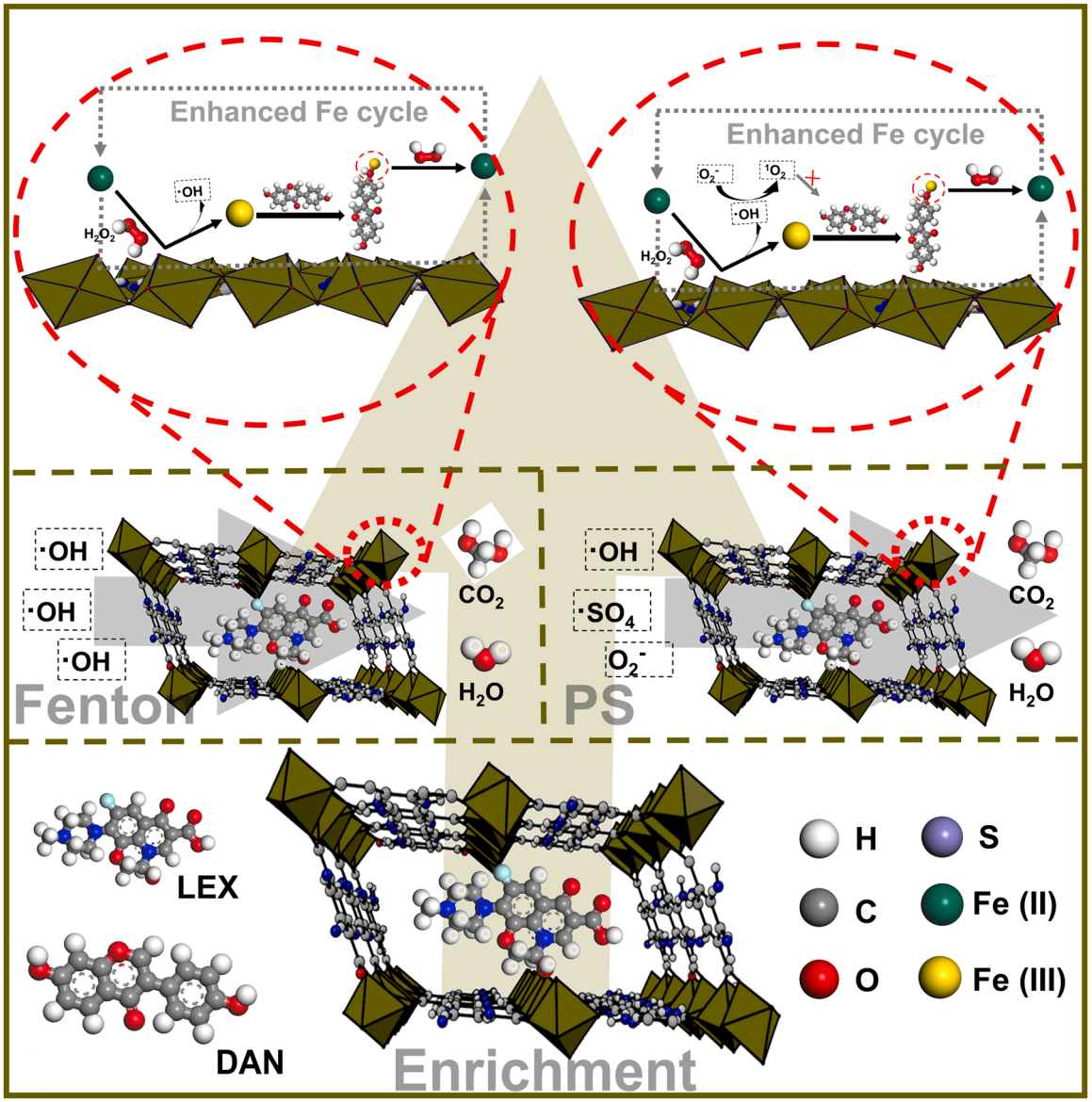

Fig. 5. the proposed Lex degradation mechanism in the Fe-MOF-DMIP/Fenton and Fe-MOF-DMIP/PS system.

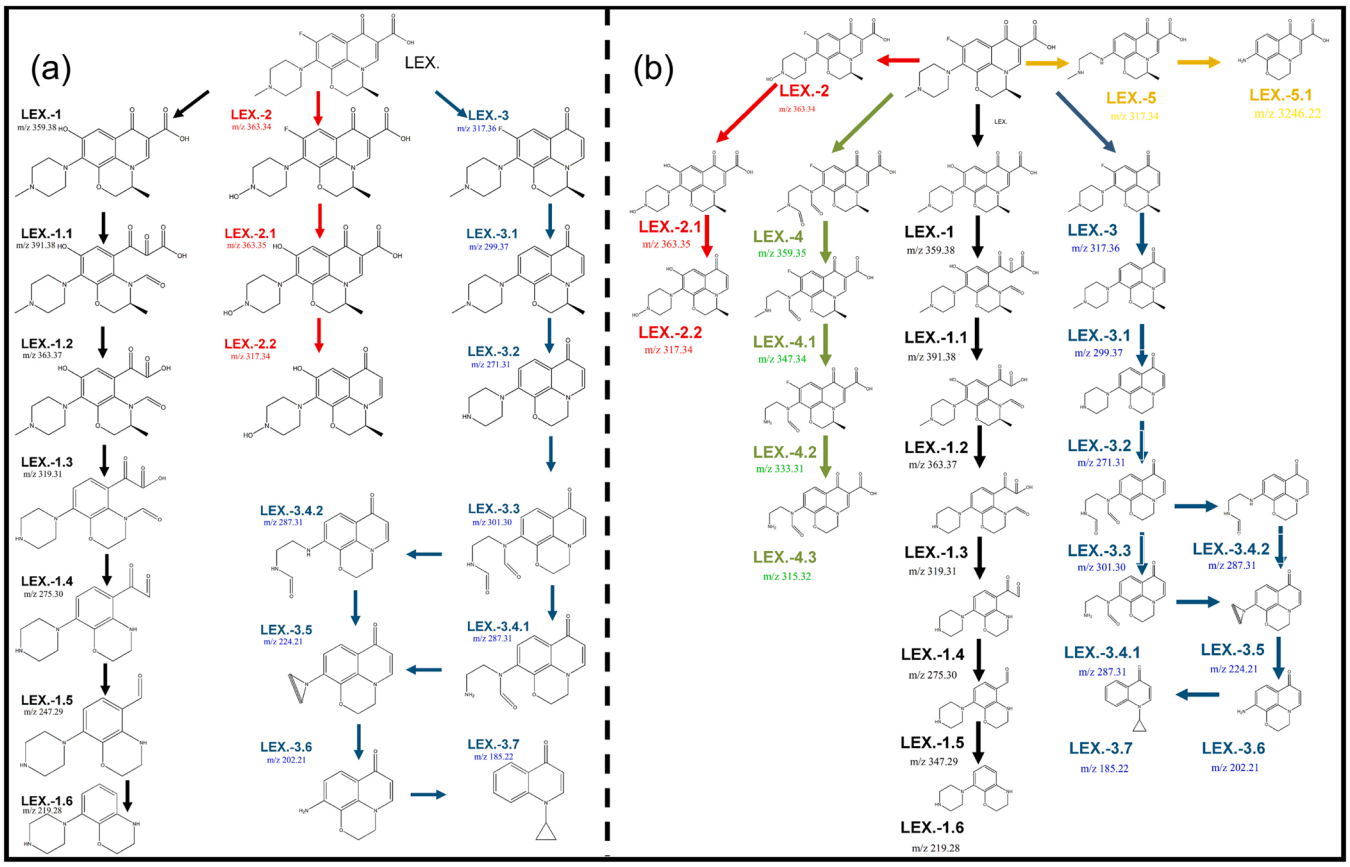

Fig. 6. Possible degradation pathways of LEX in the Fe-MOF-DMIP/Fenton system (a) and Fe-MOF-DMIP/PS system (b).

Pathway II began when the methyl group of the piperazine ring was replaced by the hydroxyl group, producing LEX-2. Then fluorine group was substituted with a hydroxyl group to form LEX-2.1. Ultimately, the intermediate product LEX-2.2 was obtained by loss of the carboxyl. In pathway III, the LEX-3 can be obtained via decarboxylation. Meanwhile, LEX-3.1 and LEX-3.2 were produced via demethylation and defluorination. Subsequently, the ring-opening reaction of piperazine ring results in the production of LEX-3.3 to LEX-3.7.

In the Fe-MOF-DMIP/PS system, in addition to the above three degradation pathways, two other degradation pathways were proposed (Fig. 6b). In pathway IV, the original pollutant LEX can be oxidized via ring-opening reaction of piperazine ring to form LEX-4. Then, the carbonyl group and methyl of piperazine ring were attacked by free radicals to produce LEX-4.1 and LEX-4.2. LEX-4.2 was further oxidized by cleaving the C-F bond on the quinolone ring to generate LEX-4.3. In pathway V, the intermediate LEX-5 was derived from the defluorination and ring-opening reaction of piperazine ring of LEX, and LEX-5.1 can be obtained via demethylation and further oxidation of piperazine rings.

3.4. pH stability, universality, anti-interference capability, reusability and economic study

3.4.1. pH stability

As shown in Fig. S12, with pH increased from 3–10, the adsorption of LEX by Fe-MOF/Fe-MOF-DMIP increased gradually, and the maximum adsorption capacity (315.31 mg g^{-1}) of Fe-MOF-DMIP appeared at pH 10. It is known that LEX exists as anion/cation or molecule at different pH values [81,53,82], but the adsorption of LEX on Fe-MOF-DMIP was not affected by anion/cation, indicating that electrostatic interaction was not the main force of LEX and Fe-MOF-DMIP. Therefore, with the increase of pH, the adsorption rate of Fe-MOF-DMIP to LEX increased significantly, it could be interpreted as that the introduction of DAN can not only improve the pH adaptability of Fe-MOF-DMIP, but also enhance the hydrogen bond interaction between Fe-MOF-DMIP and LEX. In addition, the Fe overflow concentration under different pH conditions were also detected to evaluation the pH stability of Fe-MOF-DMIP. As can be seen from Fig. S13, the concentrations of free Fe in MOF-Fe-DMIP with pH 3–11 were 101.4, 48.4, 10.7, 9.4, 7.6, 8.8, 5.6, 4.1 and 4.5 μg L^{-1}, respectively. Although the concentration of free Fe detected at pH 3 was higher than that at other pH conditions, they were all trace levels as the Fe concentration obtained by complete destruction of 4 mg Fe-MOF-DMIP was 1619.6 μg L^{-1}. These results indicated that Fe-MOF-DMIP could be stable in pH 3–11.

3.4.2. Universality and anti-interference capability

Adsorption@AOPs tests of Fe-MOF-DMIP on 11 FQs were carried out to evaluate whether the catalyst prepared by MIT@MOF strategy is suitable for the purification of a range of pollutants. As shown in Figs. 7 (a)-7(b), in the adsorption equilibrium stage, Fe-MOF-DMIP showed high enrichment ability for 11 FQs, adsorption rate was between 35.45% and 55.21%. When H_2O_2/PS was added, 74.67–83.66% (Fe-MOF-DMIP/Fenton system) and 54.80–72.16% (Fe-MOF-DMIP/PS system) FQs were removed within 30 min due to the high efficiency of oxidant utilization of Fe-MOF-DMIP. Further, FQs are almost completely degraded in Fenton system at 120 min. In summary, Fe-MOF-DMIP prepared based on MIT@MOF strategy can be used to degradation a range of FQs.

The effects of various co-existing ions (Cl^-, $H_2PO_4^-$ and HCO_3^-) and HA on LEX removal by Fe-MOF-DMIP (Fenton/PS) were investigated. As shown in Figs. 7(c)-7(d), Fe-MOF-DMIP/Fenton system can remove 95.84%, 97.81%, 95.43% and 91.87% LEX within 120 min, with the presence of low concentration of Cl^-, $H_2PO_4^-$ and HCO_3^- (1 mM) and HA (1 mg/L), respectively. And the data in Fe-MOF-DMIP/PS system were 84.84%, 83.44%, 84.37% and 83.26%. This may be due to the modification of the affinity (MIT) and oxidant catalysis ability (defectives) of

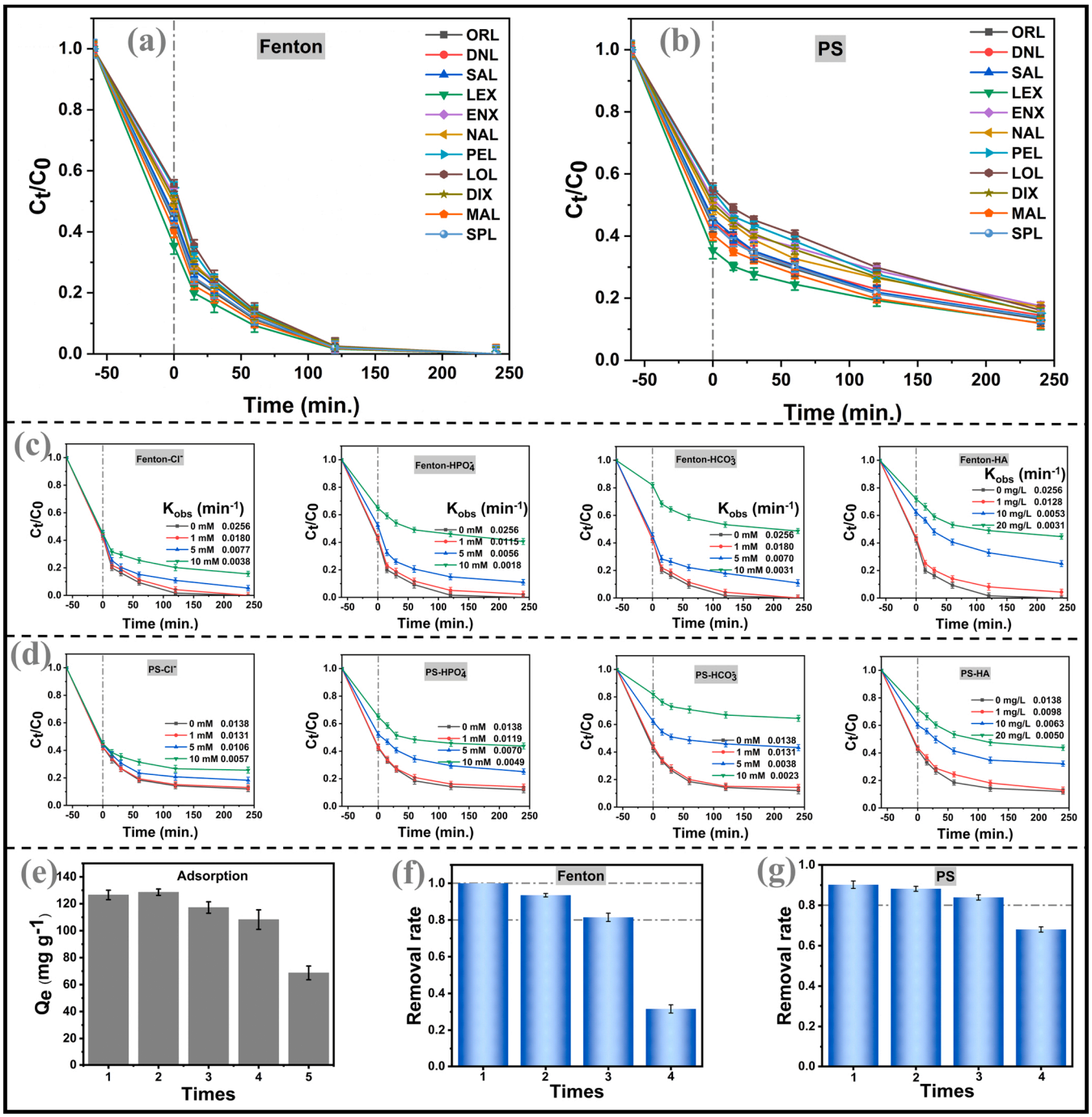

Fig. 7. FQs removal efficiency in Fe-MOF-DMIP/Fenton system (a) and Fe-MOF-DMIP/PS system (b); The effect of co-existing anions and HA on LEX degradation in Fe-MOF-DMIP/Fenton system (c) and Fe-MOF-DMIP/PS system (d); Adsorption cycle performance of Fe-MOF-DMIP (e); Adsorption@Fenton cycle performance of Fe-MOF-DMIP (f); Adsorption@PS cycle performance of Fe-MOF-DMIP (g);.

LEX by Fe-MOF-DMIP, which enriches sufficient LEX and is promptly degraded by ROS. With the concentration of ions and HA increasing to 5 mM and 10 mg/L, respectively, LEX removal rate showed a certain decrease within 120 min, reaching 89.10%, 85.09%, 82.10% and 67.09% LEX in Fe-MOF-DMIP/Fenton system and 79.27%, 70.52%, 55.09% and 65.24% in Fe-MOF-DMIP/PS system, but the degradation rate still remained above 55% at 120 min. However, when the substrates concentration increased further, the removal rate of LEX decreased significantly within 120 min, reaching 79.89%, 54.04%, 46.74% and 51.04% in Fe-MOF-DMIP/Fenton system, and 73.36%, 54.24%, 33.10% and 52.44% in Fe-MOF-DMIP/PS system. As reported, free radical scavengers (Cl^- and HCO_3^-) can react with ·OH/$SO_4^{\cdot-}$ and generate $Cl^{\cdot}$ and $CO_3^{\cdot-}$, which were weaker oxidants ($E_{Cl\cdot} = 2.09$ V) [65,68,83]. High concentrations of Cl^- and HCO_3^- could compete with LEX for ·OH and $SO_4^{\cdot-}$, resulting in a significant decrease in LEX removal. In addition, as metal complexing agent (HCO_3^- and $H_2PO_4^-$), they could coordinate with Fe defectives of Fe-MOF-DMIP, resulting an inhibition on the LEX removal process [83]. The LEX removal rates at low concentrations of HCO_3^- and $H_2PO_4^-$ were not significantly inhibited, indicating that Fe defective of Fe-MOF-DMIP was not the only adsorption interaction of Fe-MOF-DMIP to LEX, which was consistent with the previous study on adsorption mechanism. Furthermore, due to the numerous electron-rich -OH and

-COOH, the attack of Fe-MOF-DMIP by electrophilic free radicals from HA was considered to be the main factor affecting the decreasing LEX removal efficiency [65,68].

3.4.3. Reusability and economic study

First, we evaluated the sustainability of Fe-MOF-DMIP as an adsorbent alone. As was shown in Fig. 7(e), the adsorption capacity of five cycle experiments was 126.55, 128.57, 117.21, 108.26 and 68.67 mg g^{-1}, respectively. Furthermore, the leaching concentration of free Fe in the eluent of each recycle experiment and the elution efficiency of each recycle experiment (Fig. S14) indicated that the Fe-MOF-DMIP structure remained stable after four cycles of experiments. Then, we tested the cyclic performance of Fe-MOF-DMIP applied to adsorption@AOPs. As shown in the Figs. 7(f)-7(g), the LEX removal rates (Fenton oxidation) were determined as 100%, 93.49%, 81.43% and 68.43% in four cycles, respectively. Correspondingly, the results in PS oxidation were 90.19%, 88.17%, 83.90% and 82.23%. These results demonstrated the great recyclability and sustainability of Fe-MOF-DMIP in three cycles. And the gradually decreased removal rate is attributed to catalyst loss and Fe leaching with each cycle. According to the calculated RSE, the activation efficiency of Fe-MOF-DMIP for PS (69.3%) is higher than that of H_2O_2 (0.2%). Therefore, the difference in removal rate in the fourth cycle can be explained as: more Fe-MOF-DMIP is required to participate in H_2O_2 activation to achieve the similar removal effect compared to PS activation, resulting in more Fe leaching and Fe-MOF-DMIP loss in the Fe-MOF-DMIP/Fenton system. In general, Fe-MOF-DMIP showed great recyclability in adsorption alone and degradation@AOPs.

Economic study is of great significance to promote the practical application of novel functional materials in environmental purification. In Fenton oxidation and PS oxidation based on catalyst activation, oxidants and catalysts are considered to account for most of the reagent cost, according to Carra and Antoine Ghauch et al. [9,39]. In addition, considering the deviation in the actual application process, we determined that 1 L (10 mg/L) LEX can be completely degraded by 40 mg Fe-MOF-DMIP in Fe-MOF-DMIP/Fenton system, while 10 mg/L (1 L) LEX can be degraded to 1 mg/L in PS system. Therefore, the total cost (TC) for reducing LEX from 10 mg/L to 1 mg/L (1000 L, 1 m^3) calculated by Eq. S (11)-S (12) are 82.21 ¥ (12.09 $)/$m^3$ (Fenton oxidation) and 73.92 ¥ (10.87 $)/$m^3$ (PS oxidation), respectively. As shown in Table S5, due to the high activation efficiency, the preparation cost of Fe-MOFD-DMIP (especially NH_2-BDC) occupies a large part. And the relatively low yield of Fe-MOF-DMIP is also the main reason for the high cost of MOF preparation. Therefore, in order to accelerate the application of novel functional MOF materials in water environment purification, it is urgent to optimize the preparation process of ligand of Fe-MOF and improve the yield of Fe-MOF synthesis.

4. Conclusion

In conclusion, we successfully synthesized the imprinting defective Fe-MOF-DMIP using a simple one-step solvothermal method with more abundant pore structure and missing ligands defects. Compared with the Fe-MOF, Fe-MOF-DMIP exhibited a significantly excellent LEX removal efficiency both in Fenton and PS oxidation, which is mainly attributed to the enhanced the synergistic ability between LEX selectively enrichment and oxidant activation. Specifically, the temporary chelation of DAN and Fe (III) promoted the extension of ligands along the edge of DAN, leading to the formation of pore structures suitable for containing LEX, enhancing the hydrogen bond interaction and hydrophobic interaction. Subsequently, after a large amount of DAN elution, missing ligand defects were exposed, resulting in the acceleration of Fe (III)/Fe (II) cycling. Due to the synergistic adsorption and degradation technology, the enhanced enrichment capacity (Qmax was 315.31 mg·g^{-1}) and catalytic capacity (98.4% and 82.4% LEX were removed within 120 min in Fe-MOF-DMIP/Fenton and Fe-MOF-DMIP/PS system, respectively.) significantly reduced the migration distance of ROS, and improved mass transfer efficiency. Moreover, the mutual consumption between •OH, $O_2^{\bullet-}$ and $^1O_2$ has been considered to be an important reason that the degradation efficiency of LEX in Fe-MOF-DMIP/PS system is lower than that in Fe-MOF-DMIP/Fenton system, suggesting that a single ROS generation system is beneficial to improve the utilization efficiency of free radicals. It is anticipated that this work could provide a new strategy for the construction of a multifunctional catalyst with high adsorption and catalytic capacity, and provides a valuable reference for the rational selection of AOP technology based on the types of free radicals in water environment purification.

CReDiT authorship contribution statement

Ying Zhao: Conceptualization, Investigation, Calculation, Data curation, Writing – original draft. **Ruican Zhang:** Investigation, Visualization. **Jiamin Huang:** Investigation, Visualization. **Ying Zhang**: Visualization. **Bo Han:** Software. **Yupeng Ying:** Calculation, Visualization. **Min Chen**: Writing - review&editing. **Shuyu Xie:** Resources, Supervision, Writing - review&editing. **Dongmei Chen:** Conceptualization, Resources, Supervision, Writing - review&editing.

Declaration of Competing Interest

The authors declare that they have no known competing financial interests or personal relationships that could have appeared to influence the work reported in this paper.

Data Availability

Data will be made available on request.

Acknowledgements

This work was supported by the Fundamental Research Funds for the Central Universities (2662023DKPY004).

Appendix A. Supporting information

Supplementary data associated with this article can be found in the online version at doi:10.1016/j.apcatb.2023.122919.

References

[1] H. Duan, X. Hu, Z. Sun, Magnetic zeolite imidazole framework material-8 as an effective and recyclable adsorbent for removal of ceftazidime from aqueous solution, J. Hazard Mater. 384 (2020), 121406, https://doi.org/10.1016/j.jhazmat.2019.121406.
[2] M. Jeon, B.M. Jun, S. Kim, M. Jang, C.M. Park, S.A. Snyder, Y. Yoon, A review on MXene-based nanomaterials as adsorbents in aqueous solution, Chemosphere 261 (2020), 127781, https://doi.org/10.1016/J.CHEMOSPHERE.2020.127781.
[3] S. Qiu, L. Gou, F. Cheng, M. Zhang, M. Guo, An efficient and low-cost magnetic heterogenous Fenton-like catalyst for degrading antibiotics in wastewater: Mechanism, pathway and stability, J. Environ. Manag. 302 (2022), https://doi.org/10.1016/j.jenvman.2021.114119.
[4] L. Duan, H. Jiang, W. Wu, D. Lin, K. Yang, Defective iron based metal-organic frameworks derived from zero-valent iron for highly efficient fenton-like catalysis, J. Hazard Mater. 445 (2023), 130426, https://doi.org/10.1016/J.JHAZMAT.2022.130426.
[5] A. Ghauch, H. Baydoun, P. Dermesropian, Degradation of aqueous carbamazepine in ultrasonic/Fe0/H2O2 systems, Chem. Eng. J. 172 (2011), https://doi.org/10.1016/j.cej.2011.04.002.
[6] S. Al Hakim, A. Baalbaki, O. Tantawi, A. Ghauch, Chemically and thermally activated persulfate for theophylline degradation and application to pharmaceutical factory effluent, RSC Adv. 9 (2019), https://doi.org/10.1039/c9ra05362j.
[7] A. Ghauch, A.M. Tuqan, Oxidation of bisoprolol in heated persulfate/H 2O systems: Kinetics and products, Chem. Eng. J. 183 (2012), https://doi.org/10.1016/j.cej.2011.12.048.
[8] A. Ghauch, A.M. Tuqan, N. Kibbi, Naproxen abatement by thermally activated persulfate in aqueous systems, Chem. Eng. J. 279 (2015), https://doi.org/10.1016/j.cej.2015.05.067.

[9] S. Al Hakim, S. Jaber, N. Zein Eddine, A. Baalbaki, A. Ghauch, Degradation of theophylline in a UV254/PS system: Matrix effect and application to a factory effluent, Chem. Eng. J. 380 (2020), https://doi.org/10.1016/j.cej.2019.122478.
[10] M. Amasha, A. Baalbaki, A. Ghauch, A comparative study of the common persulfate activation techniques for the complete degradation of an NSAID: The case of ketoprofen, Chem. Eng. J. 350 (2018), https://doi.org/10.1016/j.cej.2018.05.118.
[11] A. Ghauch, A. Baalbaki, M. Amasha, R. El Asmar, O. Tantawi, Contribution of persulfate in UV-254 nm activated systems for complete degradation of chloramphenicol antibiotic in water, Chem. Eng. J. 317 (2017), https://doi.org/10.1016/j.cej.2017.02.133.
[12] R. El Asmar, A. Baalbaki, Z. Abou Khalil, S. Naim, A. Bejjani, A. Ghauch, Iron-based metal organic framework MIL-88-A for the degradation of naproxen in water through persulfate activation, Chem. Eng. J. 405 (2021), https://doi.org/10.1016/j.cej.2020.126701.
[13] Z.A. Khalil, A. Baalbaki, A. Bejjani, A. Ghauch, MIL88-A as a mediator for the degradation of sulfamethoxazole in PS systems: implication of solar irradiation for process improvement, Environ. Sci.: Adv. 1 (2022) 797–813, https://doi.org/10.1039/D2VA00180B.
[14] A. Ghauch, A. Tuqan, H.A. Assi, Antibiotic removal from water: Elimination of amoxicillin and ampicillin by microscale and nanoscale iron particles, Environ. Pollut. 157 (2009), https://doi.org/10.1016/j.envpol.2008.12.024.
[15] A. Ghauch, H.A. Assi, H. Baydoun, A.M. Tuqan, A. Bejjani, Fe0-based trimetallic systems for the removal of aqueous diclofenac: Mechanism and kinetics, Chem. Eng. J. 172 (2011) 1033–1044, https://doi.org/10.1016/J.CEJ.2011.07.020.
[16] A. Ghauch, H. Abou Assi, S. Bdeir, Aqueous removal of diclofenac by plated elemental iron: Bimetallic systems, J. Hazard Mater. 182 (2010), https://doi.org/10.1016/j.jhazmat.2010.05.139.
[17] A. Ghauch, H. Abou Assi, A. Tuqan, Investigating the mechanism of clofibric acid removal in Fe0/H2O systems, J. Hazard Mater. 176 (2010), https://doi.org/10.1016/j.jhazmat.2009.10.125.
[18] A. Ghauch, A. Tuqan, Reductive destruction and decontamination of aqueous solutions of chlorinated antimicrobial agent using bimetallic systems, J. Hazard Mater. 164 (2009), https://doi.org/10.1016/j.jhazmat.2008.08.048.
[19] A. Ghauch, Iron-based metallic systems: An excellent choice for sustainable water treatment, FOG - Freib. Online Geosci. 38 (2015).
[20] S. Naim, A. Ghauch, Ranitidine abatement in chemically activated persulfate systems: Assessment of industrial iron waste for sustainable applications, Chem. Eng. J. 288 (2016), https://doi.org/10.1016/j.cej.2015.11.101.
[21] A. Baalbaki, N. Zein Eddine, S. Jaber, M. Amasha, A. Ghauch, Rapid quantification of persulfate in aqueous systems using a modified HPLC unit, Talanta 178 (2018), https://doi.org/10.1016/j.talanta.2017.09.036.
[22] A. Ghauch, G. Ayoub, S. Naim, Degradation of sulfamethoxazole by persulfate assisted micrometric Fe0 in aqueous solution, Chem. Eng. J. 228 (2013), https://doi.org/10.1016/j.cej.2013.05.045.
[23] G. Ayoub, A. Ghauch, Assessment of bimetallic and trimetallic iron-based systems for persulfate activation: Application to sulfamethoxazole degradation, Chem. Eng. J. 256 (2014), https://doi.org/10.1016/j.cej.2014.07.002.
[24] S. Naim, A. Ghauch, Ranitidine abatement in chemically activated persulfate systems: Assessment of industrial iron waste for sustainable applications, Chem. Eng. J. 288 (2016), https://doi.org/10.1016/j.cej.2015.11.101.
[25] A. Wang, J. Ni, W. Wang, D. Liu, Q. Zhu, B. Xue, C.C. Chang, J. Ma, Y. Zhao, MOF Derived Co−Fe nitrogen doped graphite carbon@crosslinked magnetic chitosan Micro−nanoreactor for environmental applications: Synergy enhancement effect of adsorption−PMS activation, Appl. Catal. B. 319 (2022), 121926, https://doi.org/10.1016/J.APCATB.2022.121926.
[26] W. Xiang, Y. Zhang, Y. Chen, C.J. Liu, X. Tu, Synthesis, characterization and application of defective metal–organic frameworks: current status and perspectives, J. Mater. Chem. A Mater. 8 (2020) 21526–21546, https://doi.org/10.1039/D0TA08009H.
[27] S. Dissegna, K. Epp, W.R. Heinz, G. Kieslich, R.A. Fischer, Defective metal-organic frameworks, Adv. Mater. 30 (2018) 1704501, https://doi.org/10.1002/ADMA.201704501.
[28] H. Chen, J. Wan, Z. Yan, Y. Ma, Y. Wang, Y. Xie, J. Hou, Construction of ultra-high defective iron-based metal organic frameworks with small molecule acid regulator for enhanced degradation of sulfamethoxazole, J. Clean. Prod. 348 (2022), https://doi.org/10.1016/j.jclepro.2022.131367.
[29] L. Yang, T. Wang, Y. Zhou, B. Shi, R. Bi, J. Meng, Contamination, source and potential risks of pharmaceuticals and personal products (PPCPs) in Baiyangdian Basin, an intensive human intervention area, China, Sci. Total Environ. 760 (2021), https://doi.org/10.1016/j.scitotenv.2020.144080.
[30] W. Zhao, G. Yu, L. Blaney, B. Wang, Development of emission factors to estimate discharge of typical pharmaceuticals and personal care products from wastewater treatment plants, Sci. Total Environ. 769 (2021), https://doi.org/10.1016/j.scitotenv.2020.144556.
[31] L. Li, X. Zhao, D. Liu, K. Song, Q. Liu, Y. He, Occurrence and ecological risk assessment of PPCPs in typical inflow rivers of Taihu lake, China, J. Environ. Manag. 285 (2021), https://doi.org/10.1016/j.jenvman.2021.112176.
[32] W. Fu, J. Fu, X. Li, B. Li, X. Wang, Occurrence and fate of PPCPs in typical drinking water treatment plants in China, Environ. Geochem Health 41 (2019), https://doi.org/10.1007/s10653-018-0181-1.
[33] A. Ostovan, M. Arabi, Y. Wang, J. Li, B. Li, X. Wang, L. Chen, Greenificated molecularly imprinted materials for advanced applications, Adv. Mater. 34 (2022) 2203154, https://doi.org/10.1002/ADMA.202203154.
[34] S. Bhogal, K. Kaur, I. Mohiuddin, S. Kumar, J. Lee, R.J.C. Brown, K.H. Kim, A. K. Malik, Hollow porous molecularly imprinted polymers as emerging adsorbents, Environ. Pollut. 288 (2021), https://doi.org/10.1016/j.envpol.2021.117775.
[35] M. Yu, H. Li, J. Xie, Y. Xu, X. Lu, A descriptive and comparative analysis on the adsorption of PPCPs by molecularly imprinted polymers, Talanta 236 (2022), https://doi.org/10.1016/j.talanta.2021.122875.
[36] S. Bauer, C. Serre, T. Devic, P. Horcajada, J. Marrot, G. Férey, N. Stock, High-throughput assisted rationalization of the formation of metal organic frameworks in the iron(III) aminoterephthalate solvothermal system, Inorg. Chem. 47 (2008) 7568–7576, https://doi.org/10.1021/ic800538r.
[37] W. Tian, J. Lin, H. Zhang, X. Duan, H. Wang, H. Sun, S. Wang, Kinetics and mechanism of synergistic adsorption and persulfate activation by N-doped porous carbon for antibiotics removals in single and binary solutions, J. Hazard Mater. 423 (2022), https://doi.org/10.1016/J.JHAZMAT.2021.127083.
[38] Q. Wu, Y. Zhang, H. Liu, H. Liu, J. Tao, M.H. Cui, Z. Zheng, D. Wen, X. Zhan, FexN produced in pharmaceutical sludge biochar by endogenous Fe and exogenous N doping to enhance peroxymonosulfate activation for levofloxacin degradation, Water Res 224 (2022), 119022, https://doi.org/10.1016/J.WATRES.2022.119022.
[39] I. Carra, L. Santos-Juanes, F.G. Acién Fernández, S. Malato, J.A.S.ánchez Pérez, New approach to solar photo-Fenton operation. Raceway ponds as tertiary treatment technology, J. Hazard Mater. 279 (2014), https://doi.org/10.1016/j.jhazmat.2014.07.010.
[40] Y. Song, L. He, S. Zhang, X. Liu, K. Chen, Q. Jia, Z. Zhang, M. Du, Novel impedimetric sensing strategy for detecting ochratoxin A based on NH2-MIL-101 (Fe) metal-organic framework doped with cobalt phthalocyanine nanoparticles, Food Chem. 351 (2021), https://doi.org/10.1016/j.foodchem.2021.129248.
[41] Y. Zhang, Z. Zhang, Z. Wang, H. Pan, Y. Lin, D. Chang, Sensitive detection of prostate-specific antigen based on dual signal amplification of Fc@MgAl-LDH and NH2-MIL-101(Fe, Biosens. Bioelectron. 190 (2021), https://doi.org/10.1016/j.bios.2021.113437.
[42] S. Naghdi, A. Cherevan, A. Giesriegl, R. Guillet-Nicolas, S. Biswas, T. Gupta, J. Wang, T. Haunold, B.C. Bayer, G. Rupprechter, M.C. Toroker, F. Kleitz, D. Eder, Selective ligand removal to improve accessibility of active sites in hierarchical MOFs for heterogeneous photocatalysis, Nat. Commun. 13 (2022), https://doi.org/10.1038/s41467-021-27775-7.
[43] Z. di Wang, Y. Zang, Z.J. Liu, P. Peng, R. Wang, S.Q. Zang, Opening catalytic sites in the copper-triazoles framework via defect chemistry for switching on the proton reduction, Appl. Catal. B. 288 (2021), https://doi.org/10.1016/j.apcatb.2021.119941.
[44] H.S. Far, M. Hasanzadeh, M.S. Nashtaei, M. Rabbani, A. Haji, B. Hadavi Moghadam, PPI-dendrimer-functionalized magnetic metal-organic framework (Fe3O4@MOF@PPI) with high adsorption capacity for sustainable wastewater treatment, ACS Appl. Mater. Interfaces 12 (2020) 25294–25303, https://doi.org/10.1021/acsami.0c04953.
[45] R. Wang, H. Xu, K. Zhang, S. Wei, W. Deyong, High-quality Al@Fe-MOF prepared using Fe-MOF as a micro-reactor to improve adsorption performance for selenite, J. Hazard Mater. 364 (2019) 272–280, https://doi.org/10.1016/j.jhazmat.2018.10.030.
[46] S. Zhuang, R. Chen, Y. Liu, J. Wang, Magnetic COFs for the adsorptive removal of diclofenac and sulfamethazine from aqueous solution: Adsorption kinetics, isotherms study and DFT calculation, J. Hazard Mater. 385 (2020), 121596, https://doi.org/10.1016/j.jhazmat.2019.121596.
[47] N. Delgado, A. Capparelli, A. Navarro, D. Marino, Pharmaceutical emerging pollutants removal from water using powdered activated carbon: Study of kinetics and adsorption equilibrium, J. Environ. Manag. 236 (2019) 301–308, https://doi.org/10.1016/j.jenvman.2019.01.116.
[48] H. Fan, Y. Ma, J. Wan, Y. Wang, Z. Li, Y. Chen, Adsorption properties and mechanisms of novel biomaterials from banyan aerial roots via simple modification for ciprofloxacin removal, Sci. Total Environ. 708 (2020), 134630, https://doi.org/10.1016/j.scitotenv.2019.134630.
[49] G.K. Rajahmundry, C. Garlapati, P.S. Kumar, R.S. Alwi, D.V.N. Vo, Statistical analysis of adsorption isotherm models and its appropriate selection, Chemosphere 276 (2021), https://doi.org/10.1016/j.chemosphere.2021.130176.
[50] F. Tan, D. Sun, J. Gao, Q. Zhao, X. Wang, F. Teng, X. Quan, J. Chen, Preparation of molecularly imprinted polymer nanoparticles for selective removal of fluoroquinolone antibiotics in aqueous solution, J. Hazard Mater. (2013) 244–245, https://doi.org/10.1016/j.jhazmat.2012.11.003.
[51] G. Kaur, N. Singh, A. Rajor, Ofloxacin adsorptive interaction with rice husk ash: Parametric and exhausted adsorbent disposability study, J. Contam. Hydrol. 236 (2021), https://doi.org/10.1016/j.jconhyd.2020.103737.
[52] K.W. Goyne, J. Chorover, J.D. Kubicki, A.R. Zimmerman, S.L. Brantley, Sorption of the antibiotic ofloxacin to mesoporous and nonporous alumina and silica, J. Colloid Interface Sci. 283 (2005), https://doi.org/10.1016/j.jcis.2004.08.150.
[53] Y. Li, E. Bi, H. Chen, Effects of dissolved humic acid on fluoroquinolones sorption and retention to kaolinite, Ecotoxicol. Environ. Saf. 178 (2019) 43–50, https://doi.org/10.1016/j.ecoenv.2019.04.002.
[54] J. Li, Y. Zhou, Z. Sun, T. Cai, X. Wang, S. Zhao, H. Liu, B. Gong, Restricted access media-imprinted nanomaterials based on a metal–organic framework for highly selective extraction of fluoroquinolones in milk and river water, J. Chromatogr. A. 1626 (2020), https://doi.org/10.1016/j.chroma.2020.461364.
[55] Y. Xiang, X. Yang, Z. Xu, W. Hu, Y. Zhou, Z. Wan, Y. Yang, Y. Wei, J. Yang, D.C. W. Tsang, Fabrication of sustainable manganese ferrite modified biochar from vinasse for enhanced adsorption of fluoroquinolone antibiotics: Effects and mechanisms, Sci. Total Environ. 709 (2020), https://doi.org/10.1016/j.scitotenv.2019.136079.
[56] Z.H. Hu, Y.F. Wang, A.M. Omer, X.K. Ouyang, Fabrication of ofloxacin imprinted polymer on the surface of magnetic carboxylated cellulose nanocrystals for highly selective adsorption of fluoroquinolones from water, Int J. Biol. Macromol. 107 (2018) 453–462, https://doi.org/10.1016/j.ijbiomac.2017.09.009.

[57] W. Jiang, W.R. Cui, R.P. Liang, J.D. Qiu, Difunctional covalent organic framework hybrid material for synergistic adsorption and selective removal of fluoroquinolone antibiotics, J. Hazard Mater. 413 (2021), 125302, https://doi.org/10.1016/j.jhazmat.2021.125302.
[58] Z. Zhao, B. Liang, M. Wang, Q. Yang, M. Su, S. xuan Liang, Microporous carbon derived from hydroxyl functionalized organic network for efficient adsorption of flumequine: Adsorption mechanism and application potentials, Chem. Eng. J. 427 (2022), https://doi.org/10.1016/j.cej.2021.130943.
[59] S. Dowling, F. Regan, H. Hughes, The characterisation of structural and antioxidant properties of isoflavone metal chelates, J. Inorg. Biochem 104 (2010) 1091–1098, https://doi.org/10.1016/j.jinorgbio.2010.06.007.
[60] Y. Liu, F. Cun, D. Tian, P. Zhou, Y. Yuan, Z. Xiong, C. He, Y. Du, Z. Pan, B. Lai, Fast photo-Fenton-like oxidation in bismuth catalysis: A novel Fe(III) self-doped sodium bismuthate nanosheet, J. Hazard Mater. 435 (2022), https://doi.org/10.1016/j.jhazmat.2022.128975.
[61] H. Zhou, S. Wu, Y. Zhou, Y. Yang, J. Zhang, L. Luo, X. Duan, S. Wang, L. Wang, D.C. W. Tsang, Insights into the oxidation of organic contaminants by iron nanoparticles encapsulated within boron and nitrogen co-doped carbon nanoshell: Catalyzed Fenton-like reaction at natural pH, Environ. Int 128 (2019), https://doi.org/10.1016/j.envint.2019.04.006.
[62] Y. Bai, X. Sun, Y. Dang, S. Yu, J.J. Zhu, Y. Zhou, A self-circulating electro-fenton-like process over Fe3O4–CaO2 cathode for highly efficient degradation of levofloxacin, Chemosphere 313 (2023), https://doi.org/10.1016/j.chemosphere.2022.137520.
[63] J. Zhou, W. Liu, W. Cai, The synergistic effect of Ag/AgCl@ZIF-8 modified g-C3N4 composite and peroxymonosulfate for the enhanced visible-light photocatalytic degradation of levofloxacin, Sci. Total Environ. 696 (2019), https://doi.org/10.1016/j.scitotenv.2019.133962.
[64] Y. Pi, L. Ma, P. Zhao, Y. Cao, H. Gao, C. Wang, Q. Li, S. Dong, J. Sun, Facile green synthetic graphene-based Co-Fe Prussian blue analogues as an activator of peroxymonosulfate for the degradation of levofloxacin hydrochloride, J. Colloid Interface Sci. 526 (2018), https://doi.org/10.1016/j.jcis.2018.04.070.
[65] X. Yang, X. Xie, S. Li, W. Zhang, X. Zhang, H. Chai, Y. Huang, The POM@MOF hybrid derived hierarchical hollow Mo/Co bimetal oxides nanocages for efficiently activating peroxymonosulfate to degrade levofloxacin, J. Hazard Mater. 419 (2021), https://doi.org/10.1016/j.jhazmat.2021.126360.
[66] H. Wan, J. Yan, C. Guo, Q. Cui, W. Zhang, Synthesis of core-heteroshell structure for ZIF-67/VTM and its efficient activation of peroxymonosulfate in treatment of levofloxacin from an aqueous solution, Environ. Res 204 (2022), https://doi.org/10.1016/j.envres.2021.111986.
[67] W. Tan, Y. Ruan, Z. Diao, G. Song, M. Su, L. Hou, D. Chen, L. Kong, H. Deng, Removal of levofloxacin through adsorption and peroxymonosulfate activation using carbothermal reduction synthesized nZVI/carbon fiber, Chemosphere 280 (2021), https://doi.org/10.1016/j.chemosphere.2021.130626.
[68] Q. Zhang, X. Sun, Y. Dang, J.J. Zhu, Y. Zhao, X. Xu, Y. Zhou, A novel electrochemically enhanced homogeneous PMS-heterogeneous CoFe2O4 synergistic catalysis for the efficient removal of levofloxacin, J. Hazard Mater. 424 (2022), https://doi.org/10.1016/j.jhazmat.2021.127651.
[69] L. Jiang, Z. Wei, Y. Ding, Y. Ma, X. Fu, J. Sun, M. Ma, W. Zhu, J. Wang, In-situ synthesis of self-standing cobalt-doped nickel sulfide nanoarray as a recyclable and integrated catalyst for peroxymonosulfate activation, Appl. Catal. B. 307 (2022), https://doi.org/10.1016/j.apcatb.2022.121184.
[70] X. Cheng, H. Guo, Y. Zhang, X. Wu, Y. Liu, Non-photochemical production of singlet oxygen via activation of persulfate by carbon nanotubes, Water Res 113 (2017), https://doi.org/10.1016/j.watres.2017.02.016.
[71] Y. Pi, H. Gao, Y. Cao, R. Cao, Y. Wang, J. Sun, Cobalt ferrite supported on carbon nitride matrix prepared using waste battery materials as a peroxymonosulfate activator for the degradation of levofloxacin hydrochloride, Chem. Eng. J. 379 (2020), https://doi.org/10.1016/j.cej.2019.122377.
[72] M. Chen, C.A. Rholl, T. He, A. Sharma, K.M. Parker, Halogen radicals contribute to the halogenation and degradation of chemical additives used in hydraulic fracturing, Environ. Sci. Technol. 55 (2021), https://doi.org/10.1021/acs.est.0c03685.
[73] J. Ji, X. Yuan, Y. Zhao, L. Jiang, H. Wang, Mechanistic insights of removing pollutant in adsorption and advanced oxidation processes by sludge biochar, J. Hazard Mater. 430 (2022), https://doi.org/10.1016/j.jhazmat.2022.128375.
[74] K. MacÁková, P. Mladěnka, T. Filipský, M. Říha, L. Jahodář, F. Trejtnar, P. Bovicelli, I. Proietti Silvestri, R. Hrdina, L. Saso, Iron reduction potentiates hydroxyl radical formation only in flavonols, Food Chem. 135 (2012), https://doi.org/10.1016/j.foodchem.2012.06.107.
[75] J. Wang, C. Wang, H. Guo, T. Ye, Y. Liu, X. Cheng, W. Li, B. Yang, E. Du, Crucial roles of oxygen and superoxide radical in bisulfite-activated persulfate oxidation of bisphenol AF: Mechanisms, kinetics and DFT studies, J. Hazard Mater. 391 (2020), https://doi.org/10.1016/j.jhazmat.2020.122228.
[76] G.V. Buxton, C.L. Greenstock, W.P. Helman, A.B. Ross, Critical Review of rate constants for reactions of hydrated electrons, hydrogen atoms and hydroxyl radicals (·OH/·O− in Aqueous Solution, J. Phys. Chem. Ref. Data 17 (1988), https://doi.org/10.1063/1.555805.
[77] Y. Zhang, K. Huang, Y. Zhu, X. Chen, M. Wei, K. Yu, Kinetics and mechanisms of flumequine degradation by sulfate radical based AOP in different water samples containing inorganic anions, RSC Adv. 12 (2022), https://doi.org/10.1039/d2ra00199c.
[78] S. Lenzen, Chemistry and biology of reactive species with special reference to the antioxidative defence status in pancreatic β-cells, Biochim Biophys Acta Gen Subj. 1861 (2017), https://doi.org/10.1016/j.bbagen.2017.05.013.
[79] B. Barrios, B. Mohrhardt, P.V. Doskey, D. Minakata, Mechanistic insight into the reactivities of aqueous-phase singlet oxygen with organic compounds, Environ Sci Technol. 55 (2021), https://doi.org/10.1021/acs.est.1c01712.
[80] X. Li, Y. Hu, C. Zhang, C. Xiao, J. Cheng, Y. Chen, Electro-activating of peroxymonosulfate via boron and sulfur co-doped macroporous carbon nanofibers cathode for high-efficient degradation of levofloxacin, J. Hazard Mater. 442 (2023), 130016, https://doi.org/10.1016/J.JHAZMAT.2022.130016.
[81] J. Zhao, G. Liang, X. Zhang, X. Cai, R. Li, X. Xie, Z. Wang, Coating magnetic biochar with humic acid for high efficient removal of fluoroquinolone antibiotics in water, Sci. Total Environ. 688 (2019) 1205–1215, https://doi.org/10.1016/j.scitotenv.2019.06.287.
[82] B. Gao, Q. Chang, J. Cai, Z. Xi, A. Li, H. Yang, Removal of fluoroquinolone antibiotics using actinia-shaped lignin-based adsorbents: Role of the length and distribution of branched-chains, J. Hazard Mater. 403 (2021), https://doi.org/10.1016/j.jhazmat.2020.123603.
[83] J. Li, Y. Wan, Y. Li, G. Yao, B. Lai, Surface Fe(III)/Fe(II) cycle promoted the degradation of atrazine by peroxymonosulfate activation in the presence of hydroxylamine, Appl. Catal. B. 256 (2019), https://doi.org/10.1016/j.apcatb.2019.117782.